Journal Pre-proof

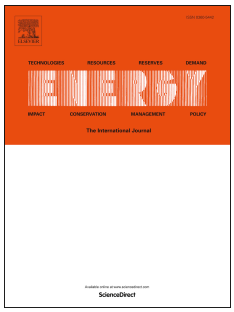

Assessment of the cost reduction potential of a novel loop-heat-pipe solar photovoltaic/thermal system by employing the distributed parameter model

Xiao Ren, Min Yu, Xudong Zhao, Jing Li, Siming Zheng, Fucheng Chen, Zhangyuan Wang, Jinzhi Zhou, Gang Pei, Jie Ji

PII: S0360-5442(19)32033-X

DOI: https://doi.org/10.1016/j.energy.2019.116338

Reference: EGY 116338

To appear in: *Energy*

Received Date: 13 February 2019

Revised Date: 23 September 2019

Accepted Date: 11 October 2019

Please cite this article as: Ren X, Yu M, Zhao X, Li J, Zheng S, Chen F, Wang Z, Zhou J, Pei G, Ji J, Assessment of the cost reduction potential of a novel loop-heat-pipe solar photovoltaic/thermal system by employing the distributed parameter model, *Energy* (2019), doi: https://doi.org/10.1016/j.energy.2019.116338.

Assessment of the cost reduction potential of a novel loop-heat-pipe solar photovoltaic/thermal system by employing the distributed parameter model

Xiao Ren[a], Min Yu[b], Xudong Zhao[b]*, Jing Li[b]**, Siming Zheng[c], Fucheng Chen[c], Zhangyuan Wang[c], Jinzhi Zhou[b], Gang Pei[a], Jie Ji[a]

[a]*Department of Thermal Science and Energy Engineering, University of Science and Technology of China, 96 Jinzhai Road, Hefei City, 230026, China*

[b]*Research Centre for Sustainable Energy Technologies, University of Hull, Hull HU6 7RX, UK*

[c]*School of Civil and Transportation Engineering, Guangdong University of Technology, 100 Waihuan Xi Road, Guangzhou, 510006, China*

*Corresponding author. Tel.: +44-01482466684, Email: xudong.zhao@hull.ac.uk

** Corresponding author. Tel.: +86-551-63607517, Email: lijing83@ustc.edu.cn

Abstract:

A novel micro-channel loop-heat-pipe solar photovoltaic/thermal (LHP- PV/T) system is developed employing the co-axial tubular heat exchanger as the condenser and upper-end liquid header with tiny holes as the liquid feeder. The design facilitates an easier connection among the solar modules. It creates the improved condensation and separate evaporation effects within the LHP. A reduced evaporator area will thereby have a minor impact on the overall heat transfer performance, leading to significant potential for cost reduction. A distributed parameter model is established and validated by experimental data. The model is then applied to analyze the cost reduction potential of the LHP-PV/T via the optimization of geometrical and structural parameters. The impact of the area reduction

on the LHP evaporator differs from that on the traditional integral heat pipe PV/T. The decrements in thermal and electrical efficiencies of the LHP- PV/T are 2.47% and 0.03% respectively when the width of heat pipes in the evaporator decreases from 26 to 10 mm. When the number of heat pipes decreases from 30 to 6, the decrements in thermal and electrical efficiencies are 4.63% and 0.12%, whilst the overall system cost drops by 28.58%, thus the cost-effectiveness of the system can be improved.

Keywords: Loop-heat-pipe; Photovoltaic/thermal; Co-axial tubular heat exchanger; Micro-channel; Cost

Nomenclature

A	area, m^2	ρ	density, kg/m^3
B	temperature coefficient, K^{-1}	σ	Stefan-Boltzman constant, $W/m^2 \cdot K^4$
Bo	Boiling number,-	τ	transmittance, -
c	specific heat capacity, J/kg·K		
d	thickness, m		
E	electrical gain, W	*Subscripts*	
G	solar irradiance, W/m^2	a	ambient, air
h	heat transfer coefficient, $W/m^2 \cdot K$	ad	adhesive layer
L	length, m	b	aluminum plate
$\dot{M}$	mass flow rate, kg/s	c	collector
M	mass, kg	e	sky
Nu	Nusselt number, -	exp	experiment
P	perimeter, m	g	glass
Pr	Prandtl number, -	h	micro-channel heat pipe
Q	heat gain, W	i	insulating layer
R	thermal resistance, $m^2 \cdot K/W$	in	water inlet
Re	Reynolds number, -	l	liquid
t	time, s	mp	maximum power
T	temperature, K	oc	open circuit
We	Weber number, -	out	water outlet
x	vapour quality, -	pv	PV module
X_{tt}	Lockhart–Martinelli parameter, -	r	working fluid

		ref	standard test condition
		sc	short circuit
Greek letters		sim	simulation
α	absorptivity, -	t	tube
ε	emissivity, -	th	thermal
η	efficiency, -	v	vapour
$(\tau\alpha)_{pv}$	effective absorption, -	vo	vapour only
ξ	covering factor, -	w	water
λ	thermal conduction, W/m·K		

1. Introduction

A loop-heat-pipe (LHP) is a form of heat pipe with good heat transfer performance, which can realize the long-distance transportation of thermal energy by using the phase change (liquid/vapour) of the working fluid in LHP [1]. LHPs typically consist of a separate heat pipe evaporator section and condenser section, a compensation chamber, a vapour line, and a liquid line. In the evaporator, the working fluid absorbs the heat and vaporizes. The vapour is transported to the condenser in which the vapour is condensed into a liquid with the same temperature and returned to the evaporator through the liquid line for replenishment. It is worth mentioning that the separated vapour and liquid lines make the installation of the LHP flexible and convenient, and are no longer limited by the orientation and distance of the heat source and heat sink [2].

At present, LHPs are widely used in thermal control of electronics, spacecraft, satellites, and cooling/heating systems. One of the main areas of application is space technology, and many devices have been successfully employed [3, 4]. In the use of the thermal regulation system of spacecraft, LHPs have the advantages of low thermal resistance, high heat transfer capacity, mechanical flexibility and good adaptability to various layout conditions. In addition, electronics and computers

are promising areas for LHP applications, revealed by the emergence of the miniature and fairly efficient devices [5, 6]. Furthermore, the application of LHPs in the field of solar water heating (SWH) system has attracted increasingly growing attention [7]. According to the research of Soin et al. [8], the problems of freezing, corrosion, and fouling in conventional solar flat plate collector systems can be eliminated by LHPs. Unlike an integral-heat-pipe (IHP) solar collector which usually has largest heat transfer irreversibility in the condenser section [9, 10] and a fixed area ratio for condenser and evaporator [11], the LHP solar system has separate evaporator and condenser. The area of the condenser section in the LHP is adjustable, then the system thereby has a large potential to improve performance, especially solar thermal efficiency.

Several studies have been conducted on the application of LHPs in SWH systems. Zhao et al. [12] proposed a novel SWH based on LHP technology for typical apartment buildings, which realized an effective collection of solar energy and long-distance transport. Zhang et al. [13, 14] introduced a solar photovoltaic (PV) LHP system for hot water and electricity generation. The electrical and thermal efficiencies of the PV/LHP system each were around 10% and 40%; whilst the overall performance coefficient (COP) was 8.7 under the given experimental conditions. Li et al. [15] presented an insert-type two-phase closed loop thermosyphon that can be applied in split-type SWHs, and the research shown that the proposed system is superior to the traditional thermosyphon in terms of start-up speed and thermal transportation limit. Aung et al. [16] studied the impact of the inclination and riser diameter on the performance in a two-phase closed loop thermosyphon SWH system. As the inclination increased, the collector efficiency increased until optimum condition, and then shown a flat trend; besides the maximum efficiency increased with the increasing of riser

diameter. He et al. [17] applied the LHP to a heat pump assisted solar façade which was an aesthetically appealing and highly efficient SWH configuration. The highest coefficient of the system can reach up to 6.14 and the average value was about 4.93.

The LHP will benefit from the use of a micro-channel evaporator. Micro-channel heat pipes (MCHPs) have been widely adopted in IHP systems. MCHPs are highly efficient heat transfer devices that rely on the phase transition of the working fluid to transport heat with the advantages of good heat transfer capacity, excellent thermal respond speed, low-pressure difference, isothermal ability, and compact structure [18]. The MCHPs comprise numerous tiny rectangular micro-channel slots with an equivalent hydraulic diameter of around 1mm. MCHPs are well suited in small space applications, such as electronics, aerospace and ultra-large-scale computing devices, where it is difficult to use large size heat transfer elements. Li et al. [19] proposed a micro-channel separate heat pipe exchanger and applied it to telecommunication stations. Diao et al. [20, 21] presented a heat exchanger based on a flat MCHP array for the ventilation of residential buildings with the advantages of compactness, lightness, and efficiency. Furthermore, the application of MCHPs in the field of the SWH system is promising. The thermal performance of the SWH system can be improved by using MCHPs in the evaporator section because MCHPs are efficient in heat absorption, convention, and transportation. At present, IHPs are favorably combined with micro-channels in the SWH system application. Deng et al. [22] and Zhu et al. [23] proposed a novel flat plate solar collector and a new compound parabolic concentrator (CPC) solar air collector based on integral MCHP technology and indicated that the system with MCHPs had the advantages of good isothermal capacity and fast thermal response speed. Hou et al. [24] studied the performance of a novel PV/T collector employing

the integral MCHP array, and the total efficiency of the collector fluctuated between 30% and 50% through the year. Modjinou et al. [25] proposed a novel PV/T system with integral MCHPs and conducted experiments and simulation studies on the system. It was found that the daily thermal and electrical efficiencies each were 50.7% and 7.6%. Besides, the MCHPs were also used in a solar-driven direct-expansion heat pump system [26]. The results indicated that the novel system could achieve an average thermal and electrical of 56.6% and 15.4%, while the average COP reached 4.7. In regard to the experience in IHP applications, improvement on the performance of LHP evaporator by micro-channels can be expected.

Similarly, there is room for improvement in the LHP condenser. In a conventional LHP-SWH system the condenser section was embedded in the water tank [27, 28]. This arrangement can reduce the power consumption of the pump, but it will not be suitable in the multiple collectors or solar arrays applications because a water tank is required for each collector and the connection among the collectors is inconvenient. Additional tanks will lead to more heat losses and higher cost. Besides, the transfer coefficient between water in the tank and working fluid in the LHP is low attributed to the natural convection. To overcome these problems, a co-axial tubular heat exchanger as the LHP condenser has been proposed by the authors. Since the evaporator and condenser sections are separated, the co-axial tubular heat exchanger for each solar module is adjustable in the area and can be easily connected in series or parallel. Water is the cooling medium and the heat collected from the solar arrays can be stored in a single big tank. The configuration and connection of the co-axial tubular heat exchangers will be illustrated in Section 2.

Above all, a combination of the co-axial tubular heat exchanger and micro-channel evaporator will be advantageous in the LHP- PV/T system application especially when a large number of solar modules are used. In the authors' previous works, the effect of the fractal geometrical parameters of wick on heat transfer capacity of the micro-channel LHP- PV/T system was studied [29]. The preliminary theoretical analysis of the system was carried out by a lumped parameter method [30]. In this method, a lumped heat capacity was assumed and one-dimensional simulation was conducted with the establishment of thermal resistance network. The system could have a 28% higher overall efficiency compared to a conventional LHP- PV/T.

The paper aims to explore the cost reduction potential of the proposed LHP- PV/T system via the optimization of the structural parameters especially the evaporator area. The novelty and contribution are:

1. A distributed parameter model with high accuracy is developed for the system. The non-uniform temperature profiles on the surface of the glass cover, PV module, aluminum plate, and MCHP shell are analyzed. The main heat transfer irreversibility in the LHP- PV/T system is revealed.
2. A micro-channel LHP- PV/T system has been recently built and is introduced. It is the first time that co-axial tubular condenser has been employed in a practical LHP- PV/T system. Experimental validation becomes possible.
3. The cost reduction potential of the proposed system is assessed for the first time. The influences of the number and width of heat pipes for the evaporator, length of the co-axial tubular condenser and thickness of aluminum plate on the system cost as well as thermal and electrical performances, are investigated.

2. Description of the LHP- PV/T system

The LHP- PV/T system comprises two parts: a LHP- PV/T collector (evaporator section) and a condenser section. As the schematic and cross-section of the novel LHP shown in Fig. 1, the condenser section is a co-axial tubular heat exchanger, wherein the cold side fluid in the inner tube is R134a and the hot side fluid in the outer tube is the water. Fig. 2 shows the structure of the evaporator section of the LHP- PV/T system. The LHP- PV/T collector is mainly composed of the glass cover, PV module, aluminum plate, micro-channel LHP, vapour header, liquid header, insulating layer, and frame. The vapour header and liquid header are located at the upper part of the collector and connected to the MCHPs. The working fluid in MCHPs absorbs the heat and vaporizes, then the vapour is accumulated at the vapour header and then sent to the condenser section in which it is condensed into liquid and returned to the liquid header. At the junction of the MCHPs and the liquid header, four tiny holes are opened on the side wall of each channel and a total of 40 holes in a MCHP. These holes allow the condensate to penetrate the pipe wall and thus maintain the downward liquid films.

Unlike the traditional LHP which has the condensed liquid returned to the bottom of the evaporator, the new LHP system makes use of an upper liquid header with the holes to deliver the liquid across the inner wall of the micro-channel evaporator, thus creating a uniformly distributed liquid film across the surface. This structure can prevent the dry-out effect inhibited into the traditional LHP, thus enhancing its heat transport capacity significantly. It should be noted that pressure difference of the liquid before and after the holes is controllable by adjusting the height of the liquid level within

the header, thus matching the heat input into the micro-channel surface and keeping a balance between the liquid supply and liquid evaporation.

The cross-section of the LHP- PV/T collector is shown in Fig. 3. The PV cells are packaged in the glass cover and laminated to the aluminum plate though the adhesive layer which is consist of tedlar-polyester-tedlar (TPT) and ethylene-vinyl-acetate (EVA), and the MCHPs are laser welded on the back of the aluminum plate. In addition, an insulating layer is employed at the bottom of the PV/T collector to reduce heat loss. The thicknesses of the glass cover, aluminum plate, and MCHP are 3.2 mm, 1.16 mm and 2 mm, respectively. There are 10 channels in each MCHP, and the width and height of a channel are 1.7 mm and 1 mm, respectively. Owing to the reduced interior size, the working fluid within the micro-channels will achieve a high vapour velocity which will generate a large shear stress force against the liquid film stuck to the inner wall of the micro-channel tube. This kind of stress force will greatly reduce the thickness of the liquid film on the channel wall [31], which will consequently lead to a high evaporation rate of the liquid on the channel wall. As a result, the micro-channel structure will result in a significantly enhanced heat transfer.

The effective radiation-collection area of the LHP- PV/T collector is 1950 mm × 950 mm. The PV/T collector is composed of 72 pieces of PV cells and 20 MCHPs. The size of a single cell is 156 mm × 156 mm, and the width and length of a single MCHP are 18 mm and 1950 mm. The diameter of each hole is 0.75mm. In the co-axial tubular heat exchanger, the inner diameter and thickness of the inner tube are 16 mm and 0.5 mm, and the inner diameter and thickness of the outer tube are 19 mm and 1 mm. The length of the co-axial tubular condenser is adjustable, and in the present system, the length

is 5 m.

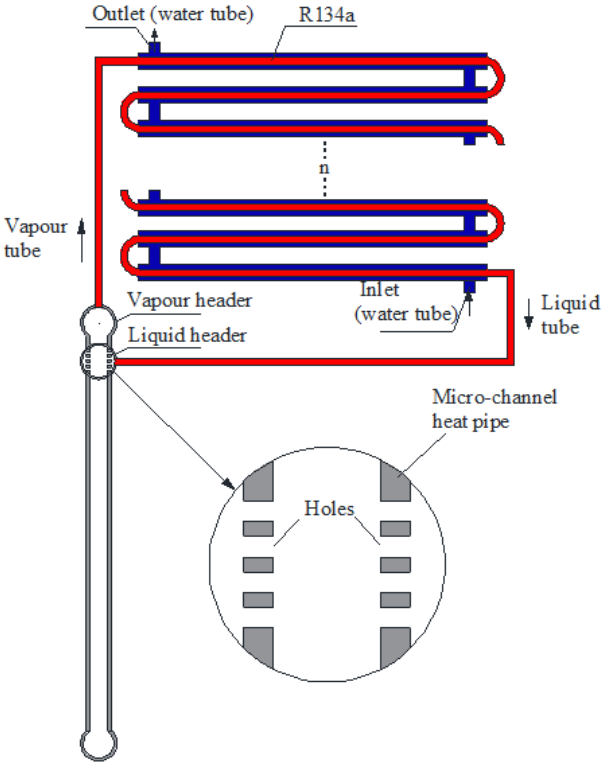

Fig. 1. Schematic and cross-section of the novel LHP.

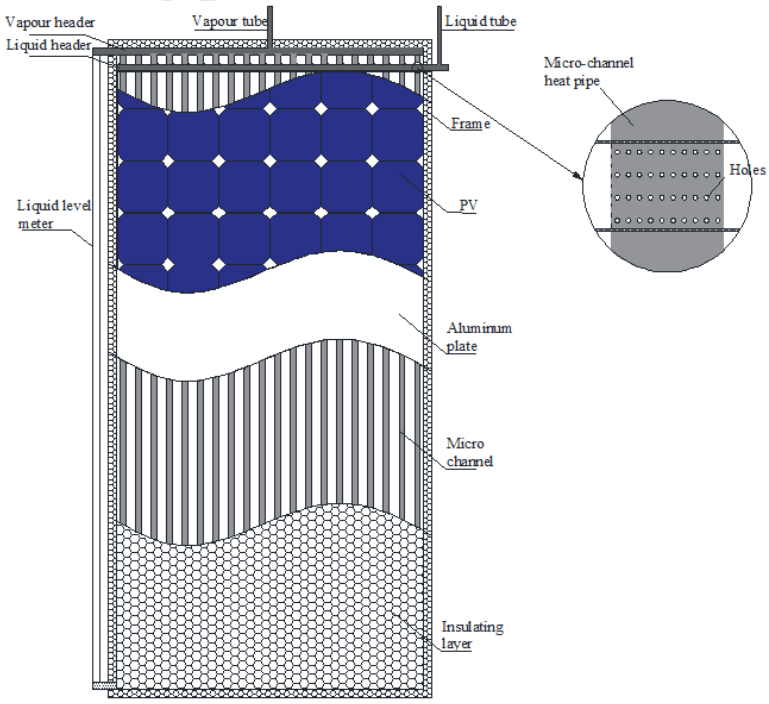

Fig. 2. Structure of the evaporator section of the LHP- PV/T system.

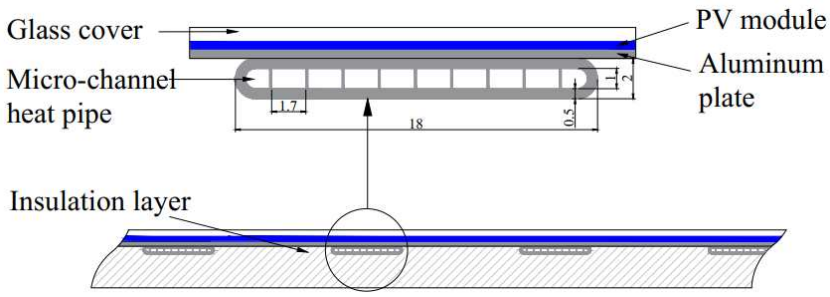

Fig. 3. Cross-section of the LHP- PV/T collector.

The condenser section in the form of the co-axial tubular heat exchanger is adjustable in the area and can easily realize the series/parallel connection of the collector arrays. Fig. 4 shows the system diagram of the LHP- PV/T collector arrays in series. It is convenient to connect the water pipes in the condenser section in series. The heat collected from the solar arrays can be stored in a single big water tank.

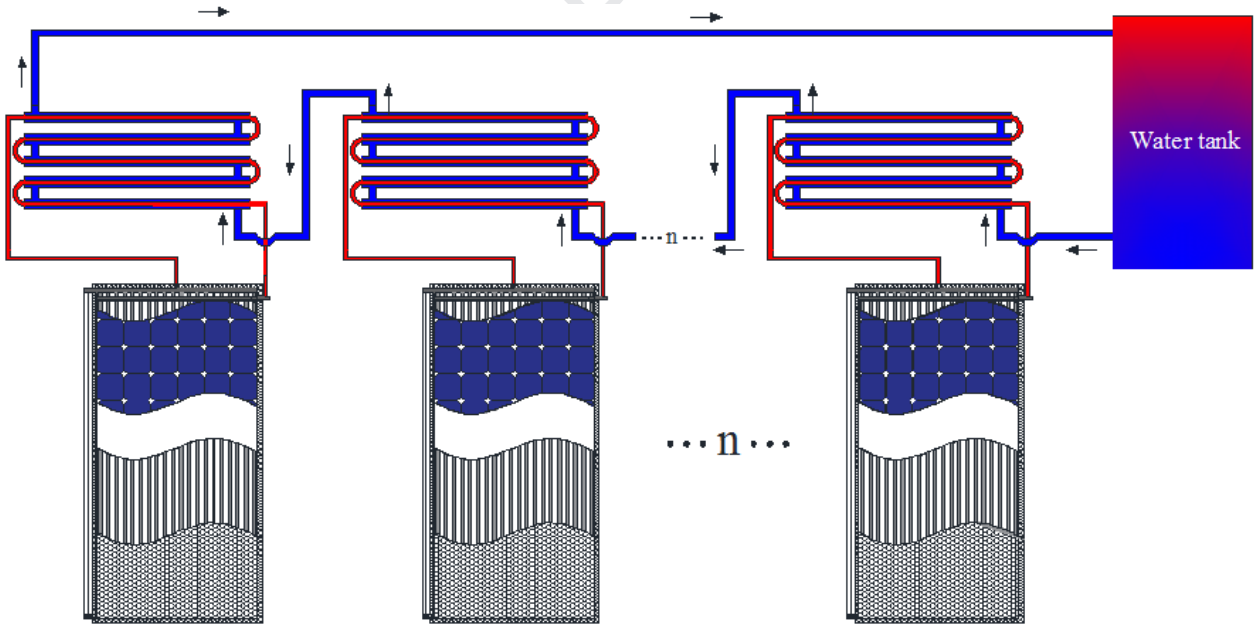

Fig. 4. Schematic of the LHP- PV/T collector arrays in series.

3. Mathematical model

3.1 Mathematic models of the LHP- PV/T system

A detailed mathematical model of the micro-channel LHP- PV/T system is developed based on the

heat transfer process by employing the distributed parameter method. The distributed parameter model describes the characteristics and dynamics of the system as a function of spatial coordinates. The established dynamic model is a partial differential model with space and time as independent variables. This dynamic model is mainly composed of heat balance equations for the following components: (1) glass cover; (2) PV module; (3) aluminum plate; (4) MCHP shell in the evaporator section; (5) working fluid in the LHP; (6) inner tube shell in the condenser section; and (7) water in the condenser section. Assumptions are made to simplify the calculation: the temperature gradients of each part along the thickness direction are negligible and the heat capacity of the adhesive layer is neglected.

For the glass cover, the heat balance equation is given as

$$d_{\mathrm{g}}\rho_{\mathrm{g}}c_{\mathrm{g}}\frac{\partial T_{\mathrm{g}}}{\partial t}=d_{\mathrm{g}}\lambda_{\mathrm{g}}\left(\frac{\partial^2 T_{\mathrm{g}}}{\partial x^2}+\frac{\partial^2 T_{\mathrm{g}}}{\partial y^2}\right)+h_{\mathrm{a}}(T_{\mathrm{a}}-T_{\mathrm{g}})+h_{\mathrm{e,g}}(T_{\mathrm{e}}-T_{\mathrm{g}})+(T_{\mathrm{pv}}-T_{\mathrm{g}})/R_{\mathrm{g,pv}}+G\alpha_{\mathrm{g}}, \quad (1)$$

where h_{a} is the convective heat transfer coefficient between the glass cover and the surrounding air ($\mathrm{W/m^2\cdot K}$); $h_{\mathrm{e,g}}$ is the radiant heat transfer coefficient between the glass cover and the sky ($\mathrm{W/m^2\cdot K}$) and $h_{\mathrm{e,g}}=\varepsilon_{\mathrm{g}}\sigma(T_{\mathrm{e}}^2+T_{\mathrm{g}}^2)(T_{\mathrm{e}}+T_{\mathrm{g}})$; T_{e} is the sky temperature (K) and $T_{\mathrm{e}}=0.0552T_{\mathrm{a}}^{1.5}$; $R_{\mathrm{g,pv}}$ is the thermal resistance between the glass cover and the PV module ($\mathrm{m^2\cdot K/W}$), expressed as $R_{\mathrm{g,pv}}=d_{\mathrm{ad}}/\lambda_{\mathrm{ad}}$.

For the PV module, the heat balance equation is expressed as

$$d_{\mathrm{pv}}\rho_{\mathrm{pv}}c_{\mathrm{pv}}\frac{\partial T_{\mathrm{pv}}}{\partial t}=d_{\mathrm{pv}}\lambda_{\mathrm{pv}}\left(\frac{\partial^2 T_{\mathrm{pv}}}{\partial x^2}+\frac{\partial^2 T_{\mathrm{pv}}}{\partial y^2}\right)+\left(T_{\mathrm{g}}-T_{\mathrm{pv}}\right)/R_{\mathrm{g,pv}}+\left(T_{\mathrm{b}}-T_{\mathrm{pv}}\right)/R_{\mathrm{b,pv}}+G\left(\tau\alpha\right)_{\mathrm{pv}}-\xi E_{\mathrm{pv}}, \quad (2)$$

where ξ is the PV cells covering factor and $\xi=A_{\mathrm{pv}}/A_{\mathrm{c}}$; $R_{\mathrm{b,pv}}$ is the thermal resistance of the

adhesive layer (black TPT and EVA) between the aluminum plate and the PV module ($m^2 \cdot K/W$) and expressed as $R_{b,pv} = d_{ad}/\lambda_{ad}$; $(\tau\alpha)_{pv}$ is the effective absorption of the PV module.

The output power of the PV module E_{pv} is calculated as

$$E_{pv} = G\tau_g\eta_{ref}\left[1-B\left(T_{pv}-T_{ref}\right)\right], \quad (3)$$

where the η_{ref} is the electrical efficiency of the PV cells under standard test condition (%); T_{ref} = 298.15 K is the temperature of the standard test condition; B is the temperature coefficient with a value of 0.002 K^{-1}.

For the aluminum plate, there are two types of energy balance equations. One type of nodes is welded with the MCHPs and has direct heat conduction with the MCHPs (connection nodes), and another type of nodes is the part of the aluminum plate between the MCHPs (middle nodes).

The heat balance equation for the connection nodes is given as

$$d_b\rho_b c_b\frac{\partial T_b}{\partial t} = d_b\lambda_b\left(\frac{\partial^2 T_b}{\partial x^2}+\frac{\partial^2 T_b}{\partial y^2}\right)+\left(T_{pv}-T_b\right)/R_{b,pv}+\left(T_h-T_b\right)/R_{b,h}\,. \quad (4)$$

The heat balance equation for the middle nodes is given as

$$d_b\rho_b c_b\frac{\partial T_b}{\partial t} = d_b\lambda_b\left(\frac{\partial^2 T_b}{\partial x^2}+\frac{\partial^2 T_b}{\partial y^2}\right)+\left(T_{pv}-T_b\right)/R_{b,pv}+\left(T_a-T_b\right)/R_{b,a}\,, \quad (5)$$

where $R_{b,h}$ is the thermal resistance of welded material between the aluminum plate and the MCHPs ($m^2 \cdot K/W$) and expressed as $R_{b,h} = d_{bh}/\lambda_{bh}$; $R_{b,a}$ is the thermal resistance between the aluminum plate and the air surrounding ($m^2 \cdot K/W$) and $R_{b,a} = d_i/\lambda_i + 1/h_a$.

For the MCHP shell in the evaporator section, the heat balance equation is expressed as

$$d_{\mathrm{h}}\rho_{\mathrm{h}}c_{\mathrm{h}}\frac{\partial T_{\mathrm{h}}}{\partial t}=d_{\mathrm{h}}\lambda_{\mathrm{h}}\left(\frac{\partial^2 T_{\mathrm{h}}}{\partial x^2}+\frac{\partial^2 T_{\mathrm{h}}}{\partial y^2}\right)+h_{\mathrm{r,h}}(T_{\mathrm{r}}-T_{\mathrm{h}})+(T_{\mathrm{b}}-T_{\mathrm{h}})/R_{\mathrm{b,h}}+\left(T_{\mathrm{a}}-T_{\mathrm{h}}\right)/R_{\mathrm{h,a}}, \tag{6}$$

where $R_{\mathrm{h,a}}$ is the thermal resistance between the MCHP shell and the air surrounding ($\mathrm{m}^2\cdot\mathrm{K/W}$), with the same value of $R_{\mathrm{b,a}}$.

The heat transfer coefficient between the MCHPs and the working fluid $h_{\mathrm{r,h}}$ is expressed as[31]

$$h_{\mathrm{r,h}}=\left(h_{\mathrm{nb}}^2+h_{\mathrm{cb}}^2\right)^{0.5}, \tag{7}$$

$$h_{\mathrm{nb}}=\left[2345\left(\mathrm{Bo}\frac{P_{\mathrm{H}}}{P_{\mathrm{F}}}\right)^{0.70}P_{\mathrm{R}}^{0.38}\left(1-x_r\right)^{-0.51}\right]\left(0.023\,\mathrm{Re}_{\mathrm{l}}^{0.8}\,\mathrm{Pr}_{\mathrm{l}}^{0.4}\frac{\lambda_{\mathrm{l}}}{D_{\mathrm{h}}}\right), \tag{8}$$

$$h_{\mathrm{cb}}=\left[5.2\left(\mathrm{Bo}\frac{P_{\mathrm{H}}}{P_{\mathrm{F}}}\right)^{0.08}\mathrm{We}_{\mathrm{l}}^{-0.54}+3.5\left(\frac{1}{X_{\mathrm{tt}}}\right)^{0.94}\left(\frac{\rho_{\mathrm{v}}}{\rho_{\mathrm{l}}}\right)^{0.25}\right]\left(0.023\,\mathrm{Re}_{\mathrm{l}}^{0.8}\,\mathrm{Pr}_{\mathrm{l}}^{0.4}\frac{\lambda_{\mathrm{l}}}{D_{\mathrm{h}}}\right), \tag{9}$$

where P_{F}, P_{H}, and D_{h} are the wetted perimeter, heated perimeter and hydraulic diameter of the MCHP (m), respectively; P_{R} is the reduced pressure; $\mathrm{Re_l}$, $\mathrm{We_l}$, $\mathrm{Pr_l}$ and Bo are liquid-only Reynolds number, Weber number, Prandtl number and Boiling number, respectively; X_{tt} is the Lockhart–Martinelli parameter based on turbulent liquid-turbulent vapour flows; x_{r} is the vapour quality.

For all the working fluid in LHP in evaporator and condenser section, the heat balance equation is expressed as

$$M_{\mathrm{r}}c_{\mathrm{r}}\frac{\partial T_{\mathrm{r}}}{\partial t}=\sum A_{\mathrm{r,h,ij}}h_{\mathrm{r,h}}\left(T_{\mathrm{h}}-T_{\mathrm{r}}\right)+\sum A_{\mathrm{r,t,ij}}h_{\mathrm{r,t}}\left(T_{\mathrm{t}}-T_{\mathrm{r}}\right), \tag{10}$$

where $A_{\mathrm{r,h,ij}}$ and $A_{\mathrm{r,t,ij}}$ are the areas of each node of the MCHP and the inner tube shell, respectively.

The convective heat transfer coefficient between the working fluid and the inner tube $h_{r,t}$ is expressed as[32]

$$h_{r,t}=\frac{\lambda_l}{D_{t,in}}\left\{\frac{0.23\mathrm{Re}_{vo}^{0.12}}{1+1.11\mathrm{X}_{tt}^{0.58}}\left[\frac{\mathrm{Ga}\cdot\mathrm{Pr}_l}{\mathrm{Ja}_l}\right]^{0.25}+\left(1-\frac{\theta_l}{\pi}\right)\mathrm{Nu}_{forced}\right\}, \tag{11}$$

$$\mathrm{Nu}_{forced}=0.0195\,\mathrm{Re}_l^{0.8}\,\mathrm{Pr}_l^{0.4}\sqrt{1.376+\frac{c_1}{X_{tt}^{c_2}}}, \tag{12}$$

where Ga and Ja_l are the Galileo number and liquid Jakob number; θ_l is the angle subtended from the top of the tube to the liquid level (°); Re_{vo} is the vapour only Reynolds number.

For the inner tube shell in the condenser section, the heat balance equation is given as

$$A_t\rho_t c_t\frac{\partial T_t}{\partial t}=A_t\lambda_t\frac{\partial^2 T_t}{\partial x^2}+P_{t,out}h_{w,t}\left(T_w-T_t\right)+P_{t,in}h_{r,t}\left(T_r-T_t\right), \tag{13}$$

where $h_{w,t}$ is the convective heat transfer coefficient between the flowing water and the inner tube ($\mathrm{W/m^2\cdot K}$); $P_{t,in}$ and $P_{t,out}$ are the inner diameter and the outer diameter of the tube (m).

For the flowing water in the condenser section, the heat balance equation is expressed as

$$A_w\rho_w c_w\frac{\partial T_w}{\partial t}=-\dot{M}_w c_w\frac{\partial T_w}{\partial x}+A_w\lambda_w\frac{\partial^2 T_w}{\partial x^2}+P_{t,out}h_{w,t}\left(T_t-T_w\right), \tag{14}$$

where $\dot{M}_w$ is the mass flow rate of the water in the condenser (kg/s).

3.2 Discretization of equations and numerical simulation

As shown in Fig. 5, half area of one MCHP and half area between two MCHPs are selected as a model (the region of differential grid partition) for simulation studies in the evaporator section. Inside the blue lines, double area of the simulation module is the display area of the temperature

distribution in Section 5.3. The detailed two-dimensional differential grids of the glass cover, the PV module, the aluminum plate, and the MCHP are divided and shown in Fig. 6. The x-axis refers to the direction along the MCHP, and the y-axis is along the direction of the header tube. As shown in Table 1, for the glass cover, the PV module and aluminum plate, the numbers of the two-dimensional discrete nodes are all 51 × 11 (i × j), and for the MCHP, the number is 51 × 5. For the water and the tube in the condenser region, 50 × 1 nodes are divided.

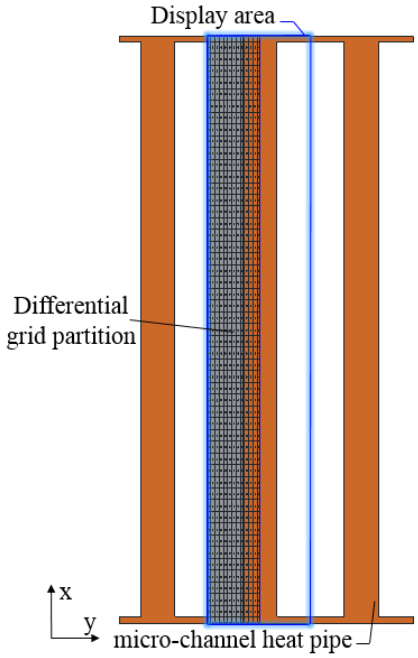

Fig. 5 Differential grid partition and display area of temperature distribution.

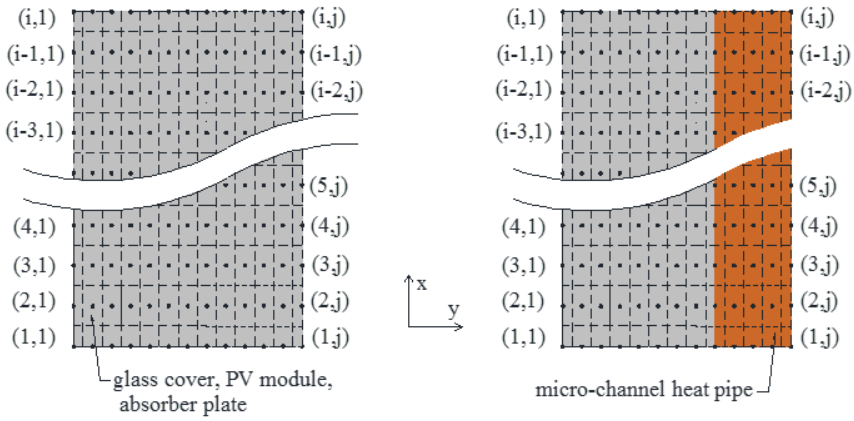

Fig. 6. Detailed differential grids of the glass cover, PV module, aluminum plate, and MCHP.

Table 1 Number of discrete node and discrete method of each component.

Component	Number of discrete node (i × j)	Discrete method
Glass cover	51 × 11	Second-order central difference scheme
PV module	51 × 11	Second-order central difference scheme
Aluminum plate	51 × 11	Second-order central difference scheme
MCHP	51 × 5	Second-order central difference scheme
Inner tube shell	50 × 1	Second-order central difference scheme
Flowing water	50 × 1	Second-order windward scheme

All the heat balance equations of the unsteady state model are solved by a fully implicit scheme, in which the heat balance equations of the glass cover, PV module, aluminum plate, MCHP shell, and inner tube shell are discretized by a second-order central difference scheme, and the heat balance equation of the water is discretized by a second-order windward scheme. The mathematical model of the LHP- PV/T system can be discretized, and the discretization of the heat balance equations is shown in Appendix.

A numerical simulation program of the model written by MATLAB is developed to predict and optimize the performances of the LHP- PV/T system. Fig. 7 shows the flow chart of the numerical simulation process. To solve the above equations, the weather data and the initial temperatures of each part are obtained from the experimental data. The time step Δt for the model is 2 s. When the differences between the two iterations of all the values are less than the acceptable error, the system is considered to reach the steady-state, and then can enter the next moment.

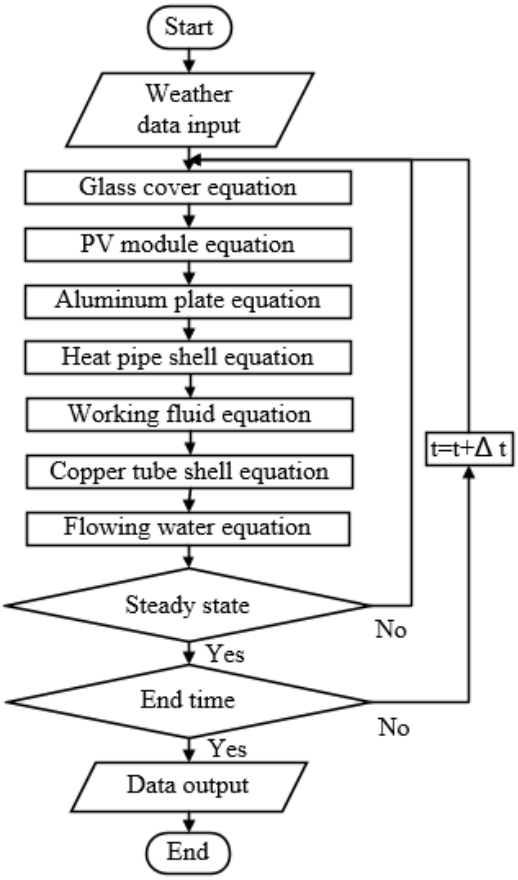

Fig. 7. Flow chart of the numerical simulation process.

3.3 Performance evaluation

The thermal efficiency is defined as the ratio of the heat gain to the incident solar irradiance.

$$\eta_{th} = \frac{Q_w}{GA_c} = \frac{c_w \dot{M}_w (T_{out} - T_{in})}{GA_c}. \tag{15}$$

A linear correlation between the instantaneous thermal efficiency η_{th} and $(T_{in} - T_a)/G$ is developed; this is expressed as [33]

$$\eta_{th} = F_R (\tau\alpha)_e - F_R U_L \frac{T_{in} - T_a}{G}, \tag{16}$$

where $F_R(\tau\alpha)_e$ is the intercept efficiency when the inlet temperature is equal to the ambient temperature; $F_R U_L$ is the coefficient of heat loss.

The electrical efficiency is expressed as

$$\eta_{\mathrm{pv}} = \frac{E_{\mathrm{pv}}}{GA_{\mathrm{pv}}}. \tag{17}$$

To evaluate the degree of agreement between the simulation and the experiment, the relative error (RE) and mean relative error (MRE) are respectively calculated by:

$$RE = \frac{X_{\mathrm{exp}} - X_{sim}}{X_{\mathrm{exp}}} \times 100\%, \tag{18}$$

$$MRE = \frac{\sum_{i=1}^{i=N} \left| X_{\mathrm{exp}} - X_{\mathrm{sim}} \right|}{\sum_{i=1}^{i=N} X_{\mathrm{exp}}} \times 100\%, \tag{19}$$

where the X_{exp} and X_{sim} are the values of the experiment and simulation, respectively.

3.4 Cost estimation

The manufacturing costs of the LHP- PV/T system are estimated by the materials costs of each component. According to the structure of the LHP- PV/T system, the manufacturing costs are expressed as the sum of costs of the glass cover, PV module, aluminum plate, MCHP, insulating layer, frame, and co-axis tubular condenser, as shown below:

$$C_{\mathrm{total}} = C_{\mathrm{g}} + C_{\mathrm{pv}} \times N_{\mathrm{pv}} + C_{\mathrm{b}} + C_{\mathrm{h}} \times N_{\mathrm{h}} + C_{\mathrm{i}} + C_{\mathrm{frame}} + C_{\mathrm{t}} \times L_t, \tag{20}$$

where the C_{g}, C_{pv}, C_{b}, C_{h}, C_{i}, C_{frame}, and C_{t} are the costs of the glass cover, a single PV cell, the aluminum plate, a single MCHP, the insulating layer, the frame and the co-axis tubular condenser per meter, and their values for a 1950 mm × 950 mm module are shown in the Table 2 [34]; N_{pv} and N_{h} are the numbers of PV cells and the MCHPs; L_{t} is the length of the co-axis tubular condenser (m).

Table 2 Manufacturing costs of each component [34].

	C_g	C_{pv}	C_b	C_h	C_i	C_{frame}	C_t
Cost (RMB)	40	5.4	61.5	15	58	61.5	40

Note: 1 RMB (Chinese Yuan) = 0.1483 US dollar

4. Experimental setup

The indoor experiments of the micro-channel LHP- PV/T system were carried out in an enthalpy-difference laboratory located in Guangzhou, where the ambient temperature can be maintained as constants. A solar simulator (PD1-ZNK1, Sunshine Technology Co., Ltd. China) was configured in the chamber to simulate solar irradiation, which is shown in Fig. 8. The instability and heterogeneity of the solar simulator are ±5%, thus the simulator can effectively simulate the solar irradiation. The collector was placed perpendicular to the horizontal position and the actual setup of the LHP- PV/T collector is shown in Fig. 9, and the solar simulator is set in parallel with the collector. Three thermocouples were arranged from the top to the bottom of the glass cover. Similarly, thermocouples were adhered to the back of the aluminum plate and heat pipe during the collector processing, and thermocouples were also placed at the water inlet and outlet of the condenser section to measure the water temperature. A water tank with storage capacity of 35 L was located near the collector. The outlet of the water tank was connected with the water inlet of the condenser section, and the inlet of the water tank was connected with the water outlet of the condenser section. The temperatures of the inlet water and outlet water were measured by platinum resistance (Pt100). A water flow meter and a circulation pump were arranged between the outlet of the water tank and the inlet of the condenser section. The experimental data such as the temperatures of the glass cover, aluminum, inlet water, outlet water, and ambient were all recorded by an Agilent data acquisition

instrument with a time interval of 30s. The experiments started about 30 minutes in advance, and the data were recorded when the system operated stably.

Fig. 8. Actual setup of the LHP- PV/T system test rig.

Fig. 9. Actual setup of the LHP- PV/T collector.

5. Results and discussions

5.1 Experimental validation

The average irradiance from the solar simulator on the surface of the LHP- PV/T collector was 560 W/m^2 and the mass flow rate of the circulating water was set as a fixed value of 0.047 kg/s. As shown in Fig. 10, the ambient temperature fluctuated between 27 °C and 28 °C, and the inlet water temperature increased from 30.3 °C to 38.3 °C during the test time.

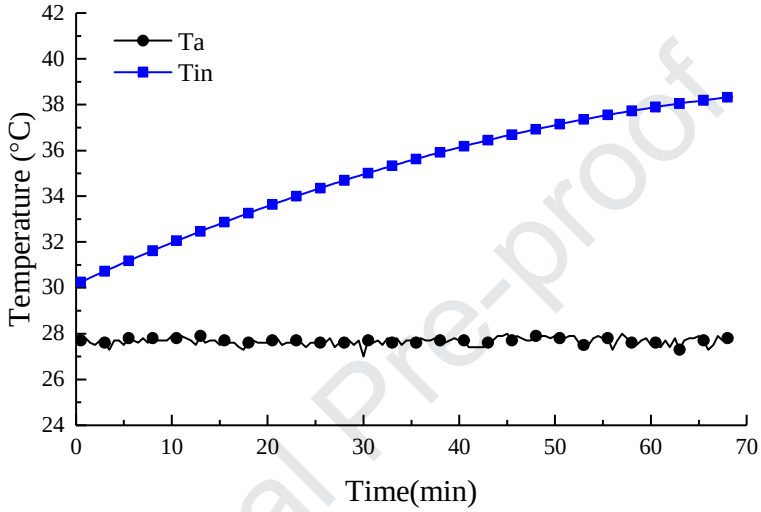

Fig. 10. Experimental ambient temperature and the inlet water temperature during the test time.

The experimental and simulation results of the glass cover temperature in the upper and lower parts are presented in Fig. 11. The temperature of the lower part is slightly higher than that of upper part. The simulated results are in good agreement with the experimental ones. Figs. 12 and 13 show the experimental and simulation results of the average temperatures of the glass cover, aluminum plate, MCHP shell, and outlet water temperature. The trends of the temperatures of these four parts were consistent with the inlet water temperature. When the inlet water temperature was 34°C, the simulation results of the temperatures of the glass cover, aluminum plate, MCHP shell, and outlet water were 36.9 °C, 37.0 °C, 36.8 °C, and 35.5 °C, whilst the experimental results were 36.8 °C, 36.9 °C, 36.8 °C, and 35.5 °C, respectively. Since the glass cover, aluminum plate, and heat pipe shell were laminated and welded together, the temperature difference between the three parts was small.

The REs and the MREs of the temperatures were shown in Table 3. The maximum RE of the four parts was only 2.49%, and the MREs were 0.57%, 0.41%, 0.56%, and 0.28%, respectively. Therefore, the accuracy and reliability of the distributed parameter model were preliminarily proved.

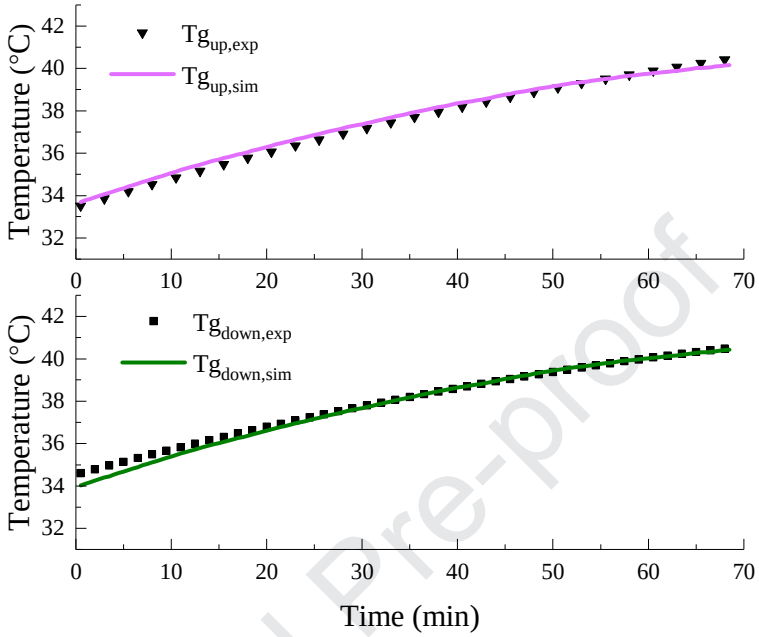

Fig. 11. Experimental and simulation results of the glass cover temperature in the upper and lower parts.

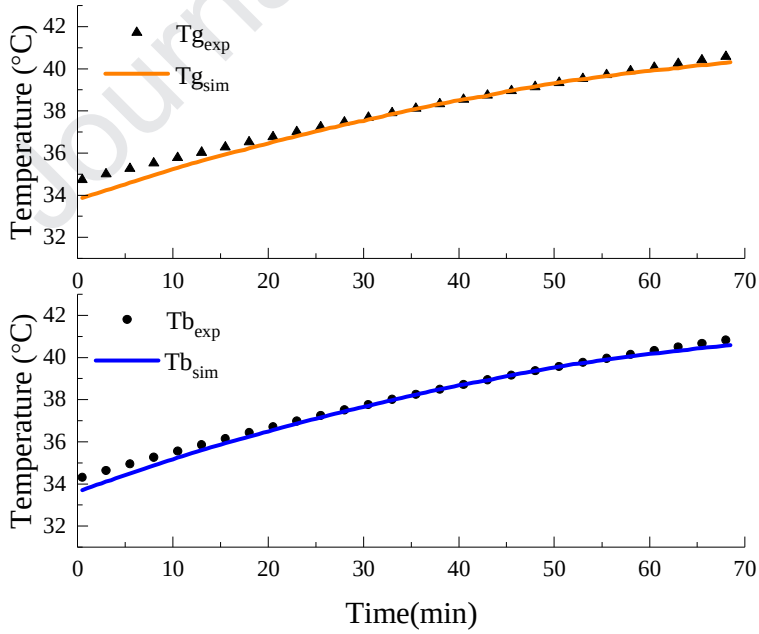

Fig. 12. Experimental and simulation results of the average temperatures of the glass cover and the aluminum plate.

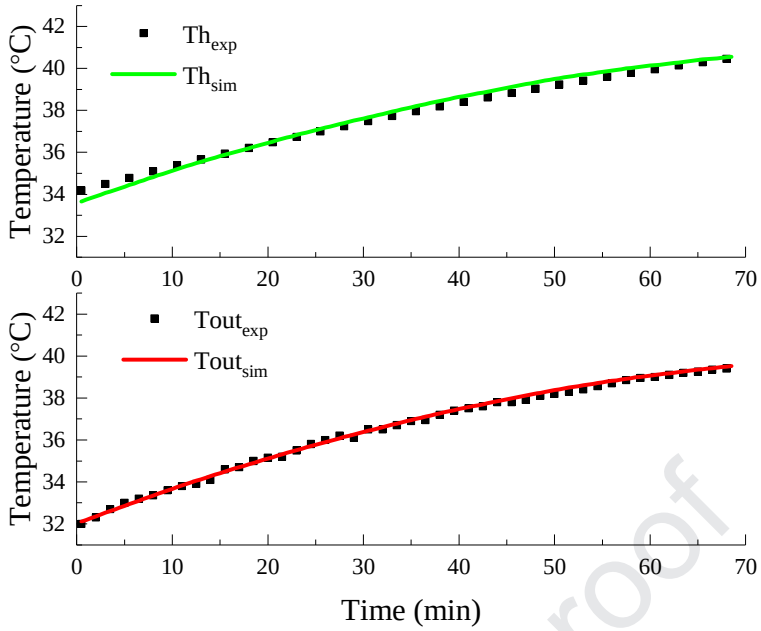

Fig. 13. Experimental and simulation results of the temperatures of the MCHP shell and the outlet water temperature.

Table 3 Comparison of the REs and the MREs between the experimental and simulation results.

	T_g	T_b	T_h	T_{out}
RE (max)	2.49%	1.76%	1.53%	0.50%
RE (min)	−0.05%	−0.02%	−0.78%	−0.71%
MRE	0.57%	0.41%	0.56%	0.28%

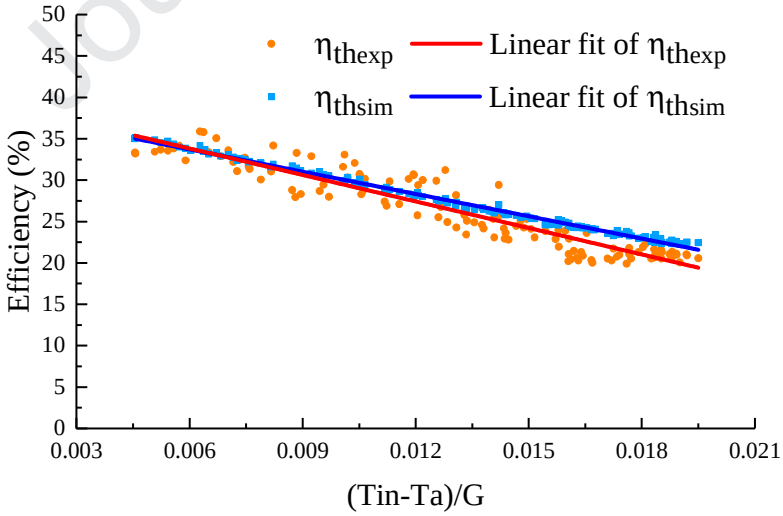

Fig. 14. Experimental and simulation results of the thermal efficiency.

The thermal efficiency η_{th} against $(T_{in}- T_a)/G$ about the LHP- PV/T system were calculated and given in Fig. 14. The experimental and simulation results of thermal efficiencies can be expressed by the

fitting formulas:

$$\eta_{\text{th,exp}} = 0.4022 - 10.665\frac{T_{\text{in}} - T_{\text{a}}}{G}, \tag{21}$$

$$\eta_{\text{th,sim}} = 0.3909 - 8.976\frac{T_{\text{in}} - T_{\text{a}}}{G}. \tag{22}$$

The experimental and simulation results of the intercept thermal efficiency were 40.22% and 39.09%, and the results of the coefficient of heat loss were 10.665 and 8.976 W/($m^2 \cdot$°C), respectively. The MRE of the experimental and simulated thermal efficiency during the test time was 7.36%.

5.2 Grid independence test

To examine the accuracy of the mathematic model, the grid independence tests are conducted from the evaporator and condenser section. The control volumes of evaporator and condenser section change from 33 to 770 and from 10 to 90, respectively. The simulation is carried out under the following fixed values: inlet water temperature of 30°C, solar irradiance of 560W/m^2, mass flow rate of 0.047 kg/s, wind velocity of 1 m/s, and air temperature of 27 °C. As shown in Fig. 15, the results reveal that the thermal and electrical efficiencies are not sensitive to the number of control volumes, especially when the control volumes of evaporator section are more than 200. Fig. 16 presents the grid independence tests of the condenser section. As the control volume increases from 10 to 90, the thermal efficiency varies from 33.62% to 38.93%, and the electrical efficiency changes from 17.08% to 17.07%. Since the code executing time will increase significantly with increasing control volumes, 561 (51 × 11) control volumes of the evaporator section and 50 (50 × 1) control volumes of the condenser section are applied in this study.

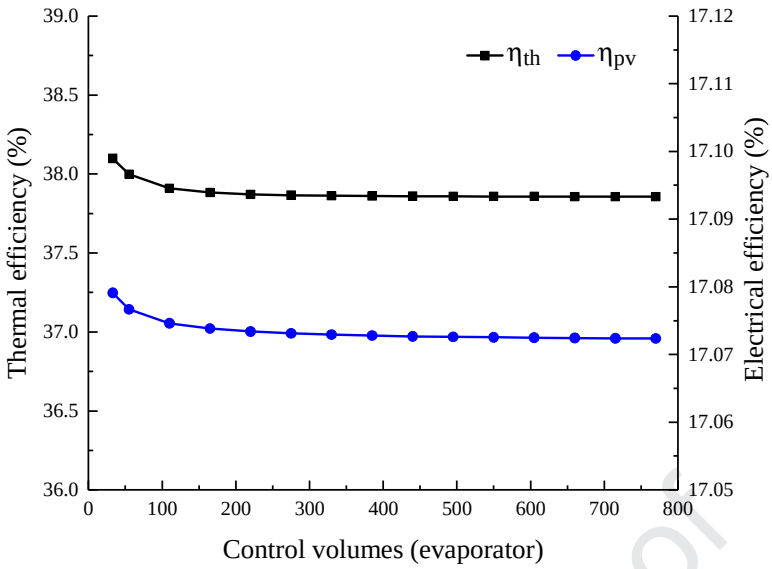

Fig.15. Grid independence tests of evaporator section.

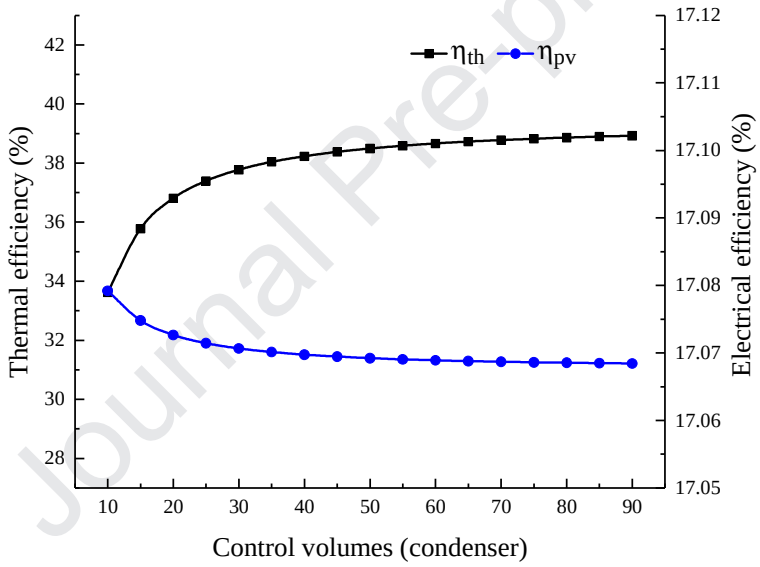

Fig. 16. Grid independence tests of condenser section.

5.3 Performance simulation and parameter optimization of the LHP- PV/T system

5.3.1 An overview of temperature distribution on the components

The simulation results of the temperature distribution of the components at the inlet water temperature of 34 °C are presented in Fig. 17. The area of a single MCHP and the area of half aluminum plate on each side of the MCHP are displayed. The temperatures of the four parts gradually decreased in the x-axis direction from the top to the bottom due to the difference in the

heat transfer coefficient of the working fluid in the MCHP. The temperature distributions of the glass cover and PV module were uniform in the y-axis direction, but the temperature of the aluminum plate connected to the heat pipe was lower than the unconnected portion on both sides of the MCHP. The average temperatures of the glass cover PV module, aluminum plate, and the single heat pipe shell were 36.8 °C, 37.4 °C, 36.9 °C and 36.8 °C, respectively, where the temperature of the PV module was the highest. When the temperature of the inlet water was 34 °C, the maximum and minimum temperatures of the PV module were 37.8 °C and 37.2 °C, respectively, and the temperature difference of the PV module in this LHP-PV/T collector was only 0.6 °C, which was much lower than that in a conventional copper tube flat plate collector. Therefore, the temperature of the PV module was relatively stable, which facilitates photoelectric conversion.

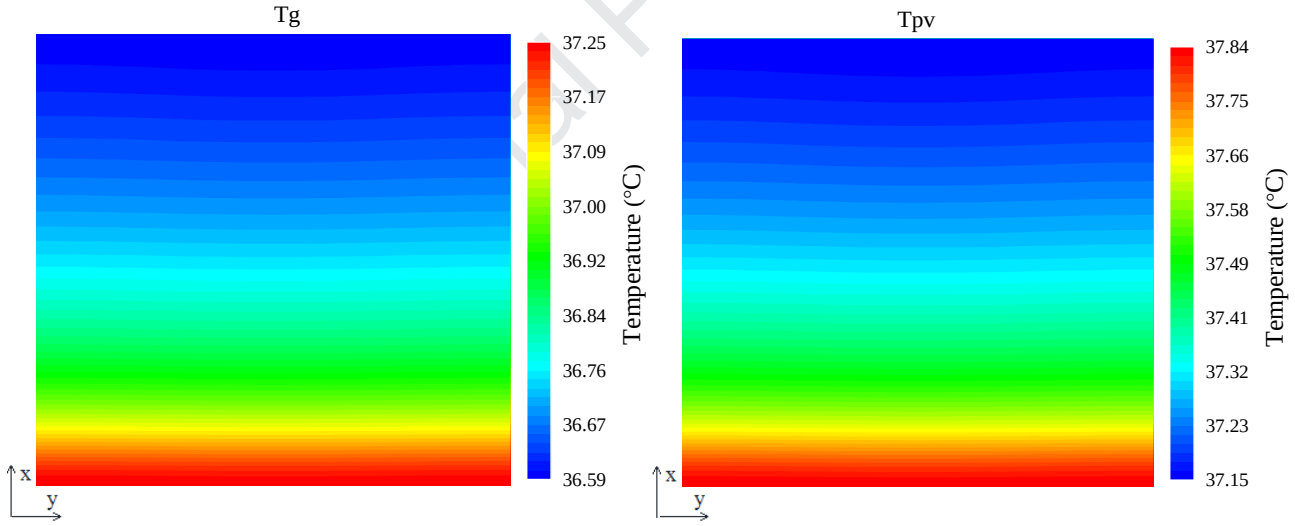

(a) (b)

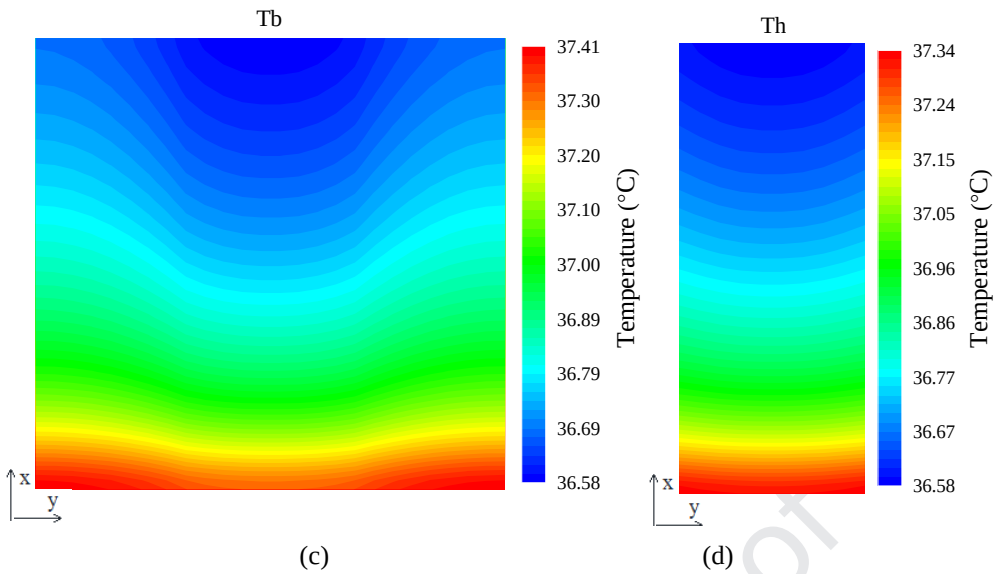

Fig. 17. The temperature distributions at inlet water temperature of 34 °C: (a) the glass cover; (b) the PV module; (c) the aluminum plate; (d) a single heat pipe shell.

Fig. 18 presents the simulation results of the thermal and electrical efficiency of the LHP- PV/T system. As the temperature of the inlet water increased, the thermal efficiency showed a downward trend, which was caused by the increased heat loss to the environment. The PV/T had a large heat loss coefficient as there was no air gap between the absorber and the glass cover. Furthermore, the high-temperature coefficient of the PV cells led to a reduction in electrical efficiency. As the temperature of the inlet water increased from 30.3 °C to 38.3 °C, the thermal efficiency decreased by 12.79%, from 35.12% to 22.33%, and the electrical efficiency decreased from 17.11% to 16.63%. When the temperature of the inlet water was 34 °C, the thermal efficiency and electrical efficiency of the LHP- PV/T system were 28.75% and 16.89%, respectively.

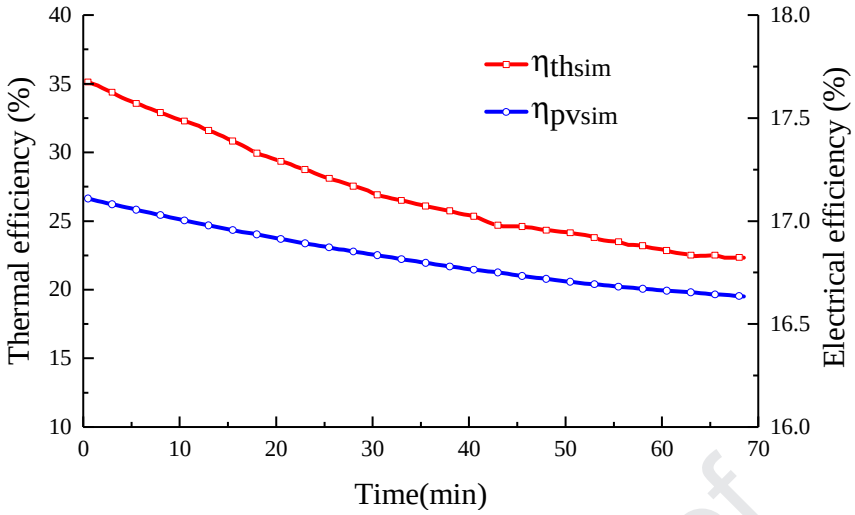

Fig. 18. Simulation results of the thermal efficiency and electrical efficiency of the LHP- PV/T system.

5.3.2 Influence of the number of heat pipes

The number and width of the MCHP and the length of the co-axial tubular condenser are important parameters that affect the performance and manufacturing costs of the LHP- PV/T system. On the basis of the experimentally validated mathematical model, the impacts of these parameters are studied in following sections. The simulation conditions are similar to those in Section 5.2.

Fig. 19 shows the effects of different numbers of heat pipe on the thermal and electrical efficiencies of the LHP- PV/T system. The length of the co-axial tubular condenser and the width of the heat pipe are the fixed values of 5 m and 18 mm. With the decrease in the number of heat pipes, both thermal and electrical efficiencies show a downward trend, and the decrements become more significant at a lower number. When the number of heat pipes is reduced from 30 to 6, the thermal efficiency decreases from 39.22% to 34.59% and the decrement is only 4.63% which is not appreciable. The main reason is that the decrease of the evaporator area results in a larger thermal resistance between the working fluid and PV/T absorber but the enlarged thermal resistance is still not predominant in the LHP- PV/T system. The effect of the number of heat pipes on electrical performance is weaker than that on the thermal performance. For instance, as the number of heat pipe decreases from 30 to 6,

the decrements in the electrical gain and electrical efficiency are only 1.11 W and 0.12%, respectively.

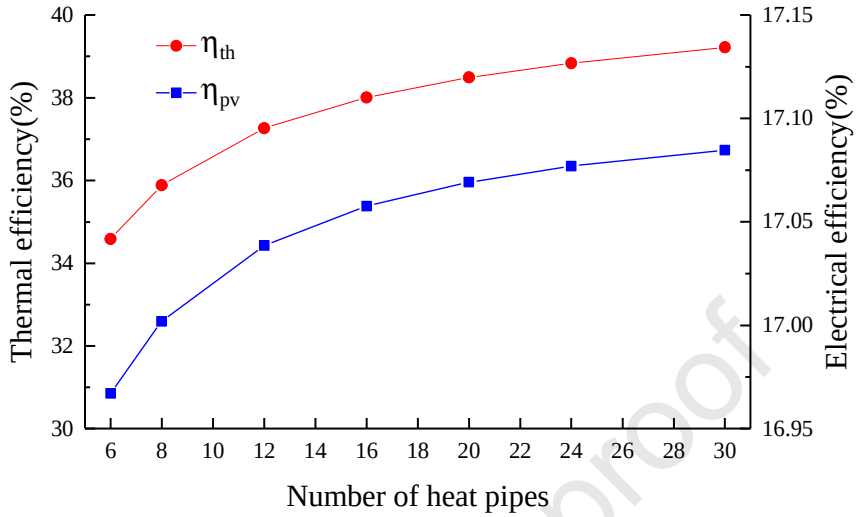

Fig. 19. Effects of different numbers of heat pipe on the thermal efficiency and electrical efficiency of the LHP- PV/T system.

Fig. 20 shows the temperature distributions of the single heat pipe shell and the aluminum plate at different numbers of heat pipes. The temperature of the MCHP shell gradually increases from the top to the bottom, which is caused by the difference in heat transfer coefficient between the working fluid and the MCHP shell. The temperature of the aluminum plate connected to the heat pipe is lower than the temperature of the aluminum plate on both sides. Moreover, as the number of heat pipes decreases, the temperature difference between the aluminum plate connected to the heat pipe and the aluminum plate on both sides becomes larger. When the numbers of heat pipes are 6, 12, 20 and 30, the average temperatures of the aluminum plate are 35.72 °C, 34.68 °C, 34.24 °C and 34.01 °C, and the average temperatures of the MCHP shell are 34.87 °C, 34.46 °C, 34.18 °C and 33.99 °C, respectively. The temperature difference between the aluminum plate and the heat pipe are 0.85 °C, 0.22 °C, 0.06 °C, and 0.02 °C. Therefore, when the number of heat pipes is small, the heat is not well dissipated in the aluminum plate unconnected to the heat pipe in the collector, and the temperature

difference between the aluminum plate and the heat pipe is large, which means that the heat cannot be utilized effectively by the heat pipe, thus resulting in a low thermal efficiency. When the numbers of heat pipes are 6, 12, 20 and 30, the temperature differences between the highest temperature and the lowest temperature of the aluminum plate are 1.55 °C, 1 °C, 0.87 °C, 0.79 °C, respectively. Therefore, as the number of heat pipes gets larger, the temperature distribution of the aluminum becomes more uniform. In addition, as the number of heat pipes increases, the temperature of PV module decreases, and thus the electrical efficiency and electrical gain increase due to the negative temperature coefficient of the PV module.

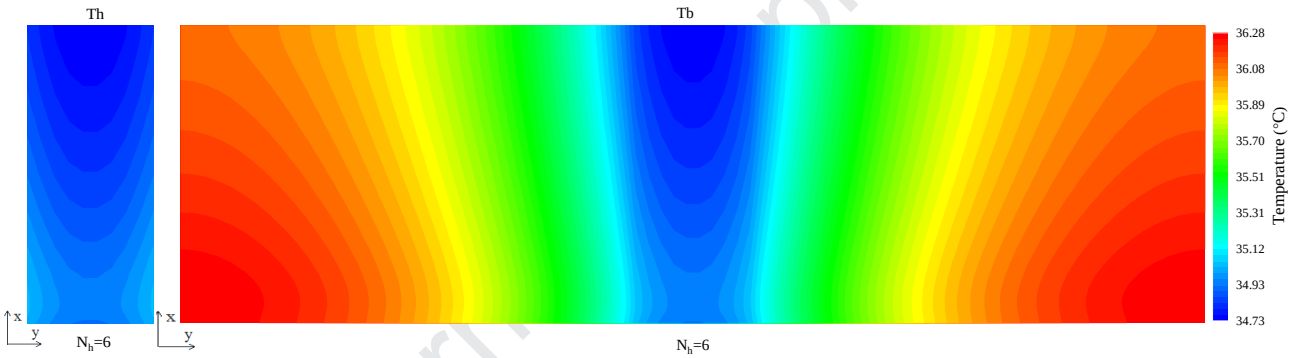

(a)

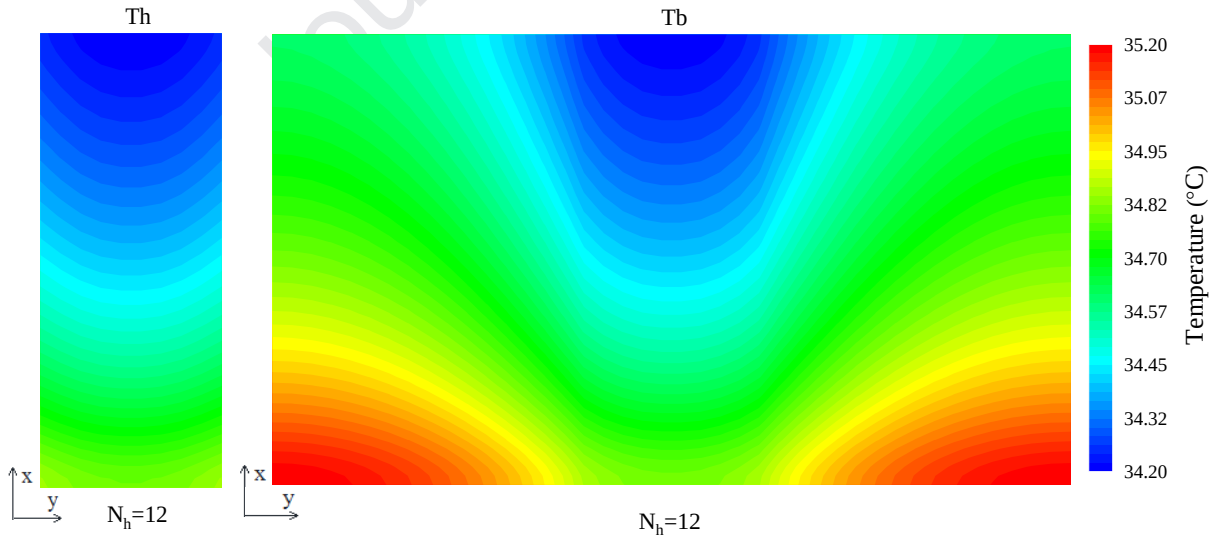

(b)

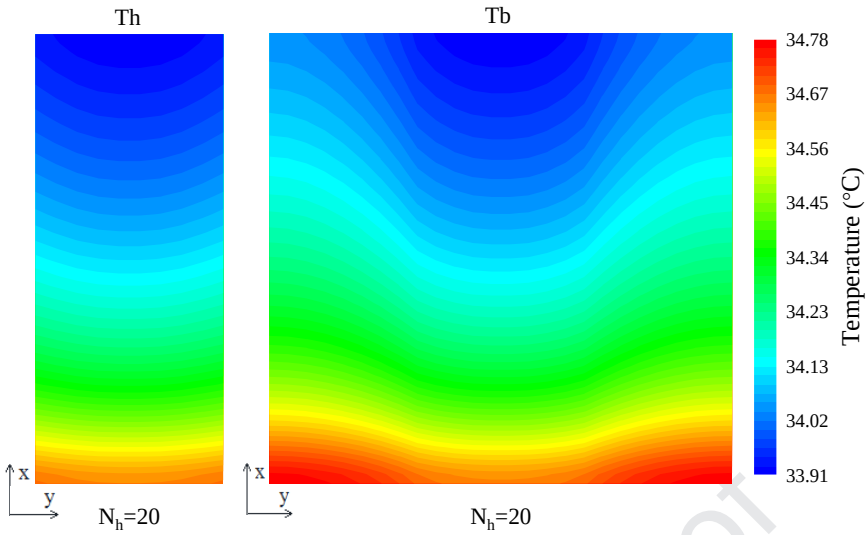

(c)

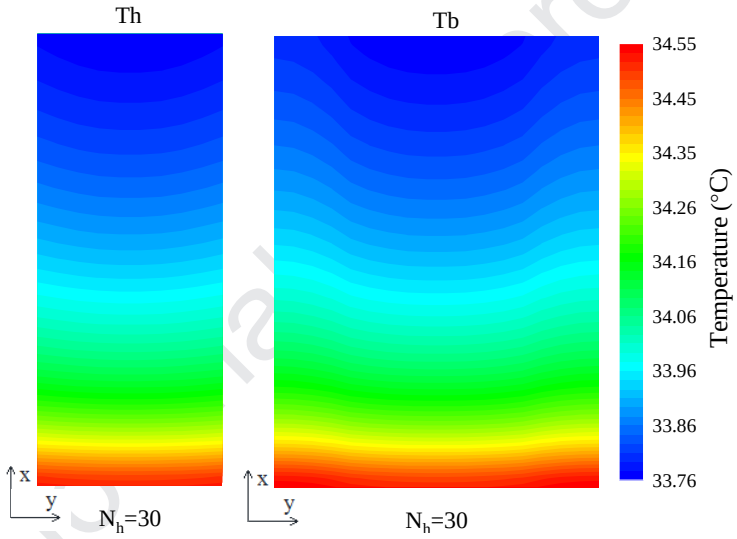

(d)

Fig. 20. Temperature distributions of the single heat pipe shell and the aluminum plate at different numbers of heat pipes: (a) N_h=6; (b) N_h=12; (c) N_h=20; (d) N_h=30.

5.3.3 Influence of the width of the heat pipe

Fig. 21 shows the effects of different widths of heat pipe on the thermal and electrical performance of the LHP- PV/T system. The length of the co-axial tubular condenser and the number of heat pipes are fixed values of 5 m and 20, respectively. As the width of the heat pipe decreases, both thermal and electrical efficiencies drop. When the widths of heat pipe are 26 mm, 18 mm and 10 mm, the thermal efficiencies are 39.33%, 38.49%, and 36.86%, respectively, and these decrements are

inconspicuous. The influence of the width of heat pipe on electrical performance is much weaker than that on the thermal performance. For example, as the width of heat pipe decreases from 26 mm to 10 mm, the decrement in the electrical efficiency is only 0.03%, from 17.08% to 17.05%.

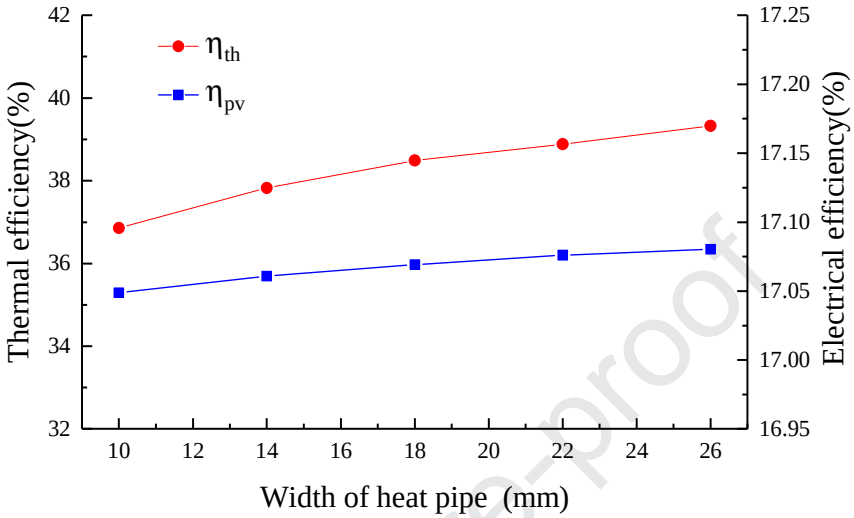

Fig. 21. Effects of different widths of heat pipe on the thermal efficiency and electrical efficiency of the LHP- PV/T system.

Fig. 22 shows the temperature distributions of the single heat pipe shell and the aluminum plate at different widths of the heat pipe. When the widths of heat pipe are 10 mm, 18 mm and 26 mm, the average temperatures of the aluminum plate are 34.53 °C, 34.24 °C and 34.07 °C, and the average temperatures of the MCHP are 34.43°C, 34.18 °C, 34.04 °C. The temperature differences between the highest temperature and the lowest temperature of the aluminum plate are all about 0.8 °C, but as the width increases, the temperature difference of the aluminum plate on the y-axis is reduced.

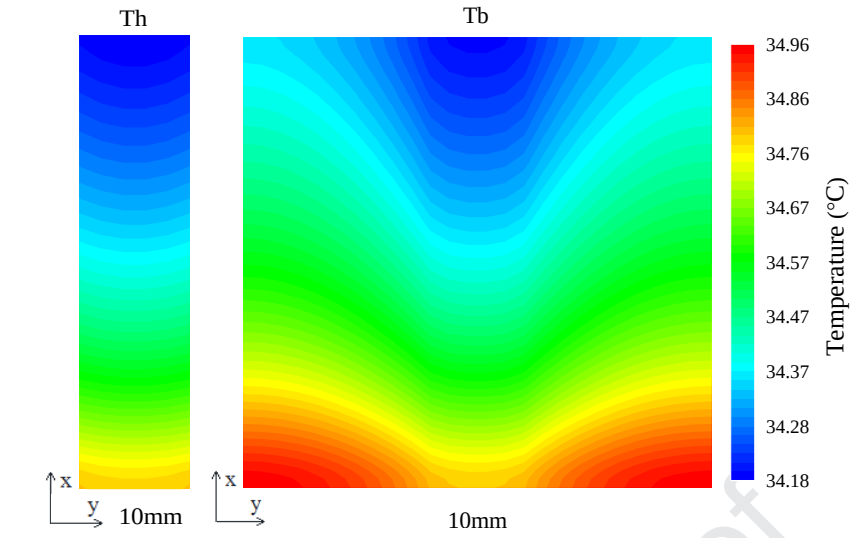

(a)

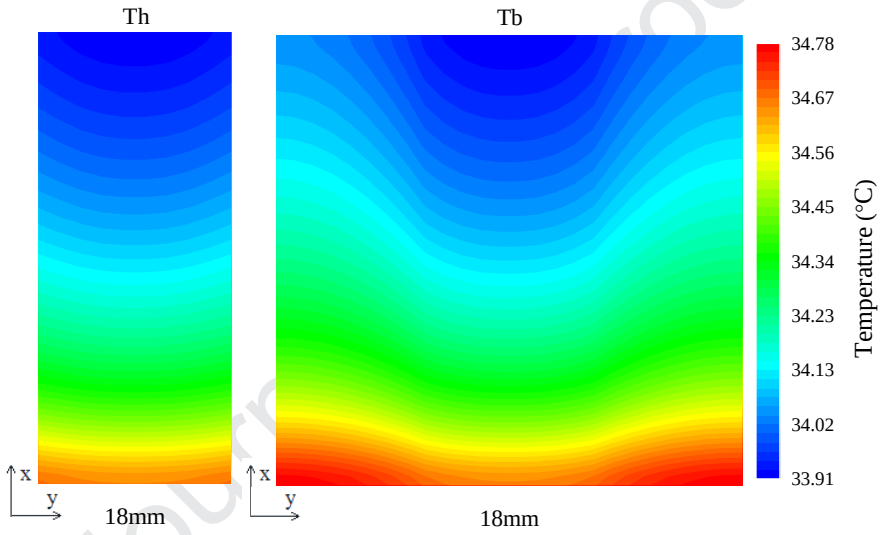

(b)

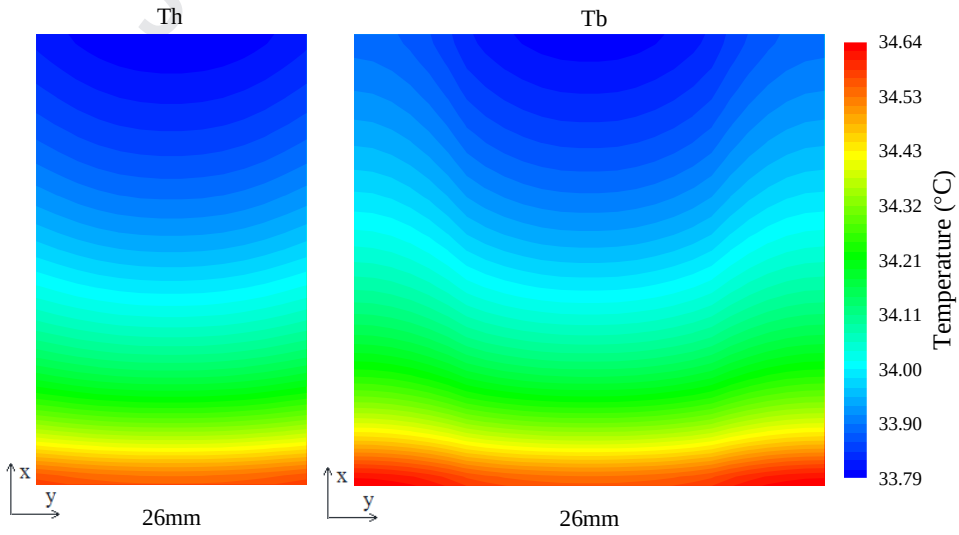

(c)

Fig. 22. Temperature distributions of the single heat pipe shell and the aluminum plate at different widths of heat pipe: (a) 10 mm; (b) 18 mm; (c) 26 mm.

5.3.4 Influence of the thickness of the aluminum plate

To evaluate the effect of the thickness of the aluminum plate on the thermal and electrical performances, other parameters are set as fixed values. It is clear from Fig. 23 that both thermal efficiency and electrical efficiency of the LHP- PV/T system increase under the different thickness of the aluminum plate at elevated number of the heat pipes. Moreover, the thermal and electrical efficiencies get higher with the increment of the aluminum plate thickness, and the influence of number of the heat pipe on the thermal and electrical performances become weaker. When the number of the heat pipe is 6, as the thickness of the aluminum plate increases from 0.58 mm to 2.32mm, the thermal efficiency increases by 1.86%, from 33.56% to 35.42%. By contrast, when the number of the heat pipe is 30, the thermal efficiency only increases by 0.31%, from 39.03% to 39.34%.

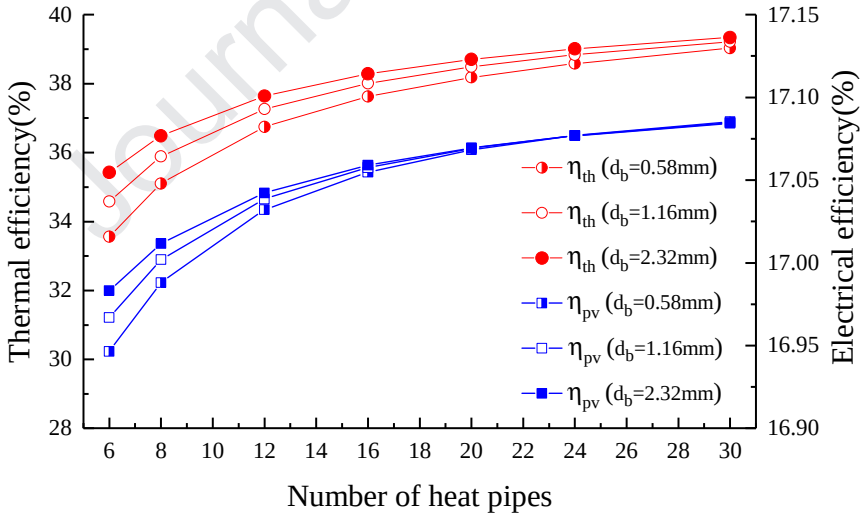

Fig. 23. Effects of the thickness of the aluminum plate on the thermal efficiency and electrical efficiency of the LHP-PV/T system.

When the number of the heat pipe is 20, the temperature distributions of the single heat pipe shell and the aluminum plate at different thicknesses of the aluminum plate are shown in Fig. 24. At the thicknesses of the aluminum plate of 0.58 mm, 1.16 mm, and 2.32 mm, the average temperatures of

the aluminum plate are all around 34.24 °C, and the temperature differences between the highest temperature and the lowest temperature of the aluminum plate are 0.97 °C, 0.87 °C, 0.8 °C, respectively. Besides, as the thickness increases, the temperature difference of the aluminum plate on the direction of y-axis is reduced. Therefore, the thicker the aluminum plate, the more uniform the distribution of the aluminum plate. It also indicates that the heat transfer in the portion of aluminum plate unconnected to the heat pipe at a small thickness of the aluminum plate is inefficient, resulting in low thermal efficiency.

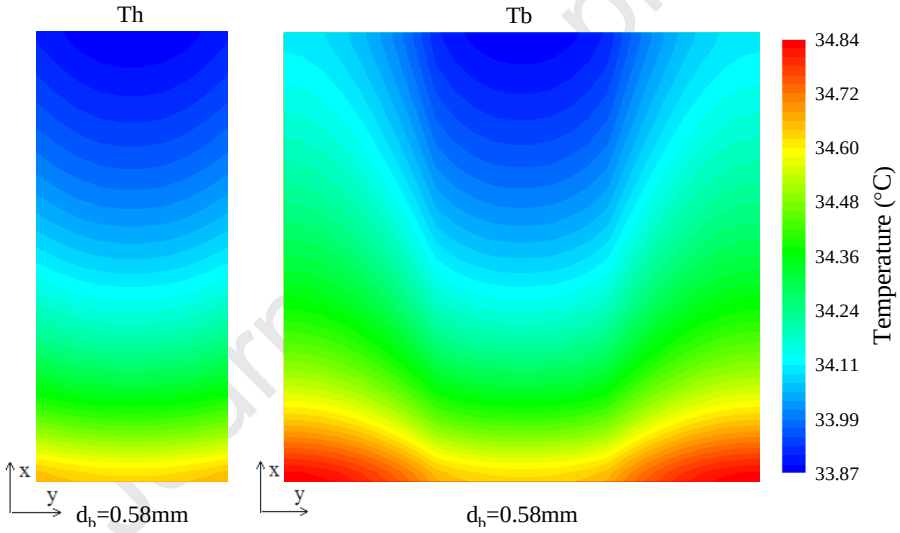

(a)

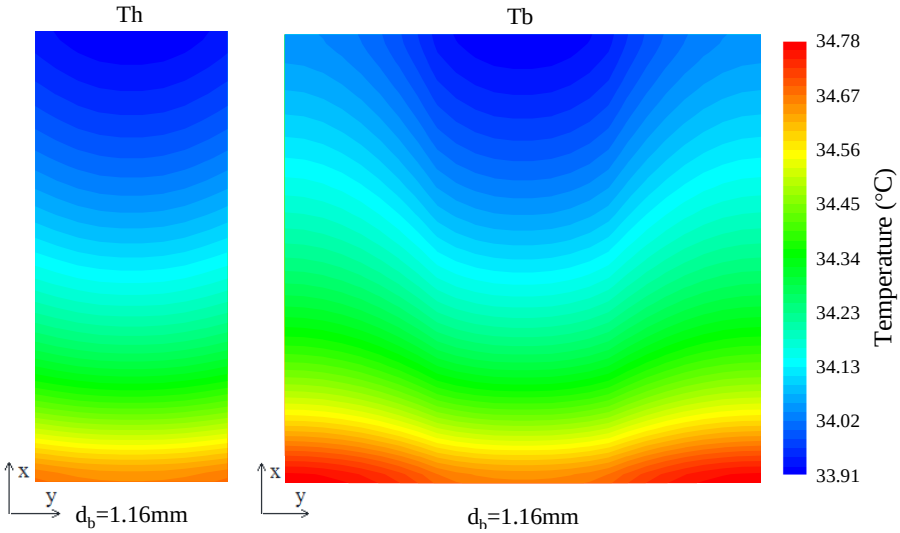

(b)

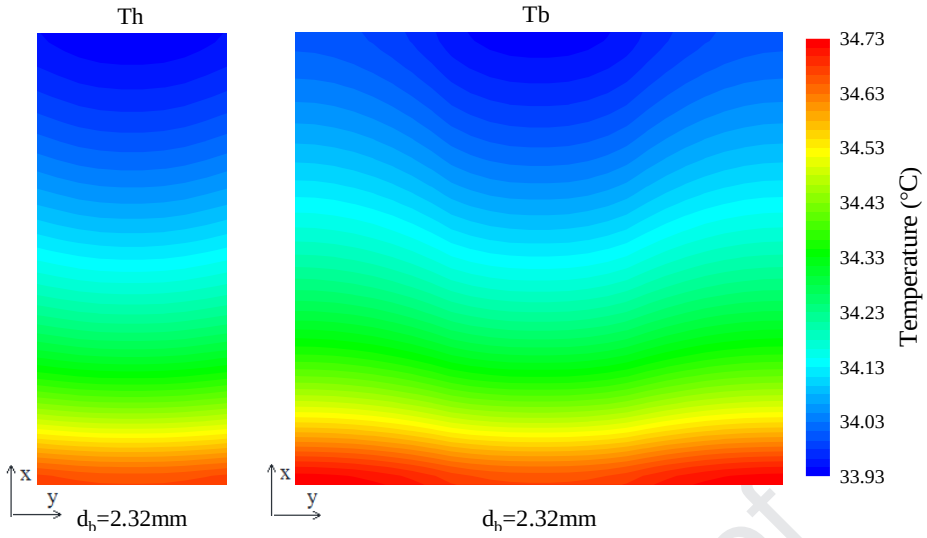

(c)

Fig. 24. Temperature distributions of the single heat pipe shell and the aluminum plate at different thicknesses of the aluminum plate: (a) d_b=0.58 mm; (b) d_b=1.16 mm; (c) d_b=2.32 mm.

5.3.5 Influence of the length of the co-axial tubular condenser

Fig. 25 illustrates the thermal and electrical efficiencies of the LHP- PV/T system under different lengths of the co-axial tubular condenser. The decreased length of the co-axial tubular condenser shows a negative influence on the thermal and electrical performances. In particular, when the length of the co-axial tubular condenser decreases from 4 m to 1 m, the performance shows a significant decline. As the length of the co-axial tubular condenser decreases from 10 m to 1 m, the thermal efficiency drops from 40.37% to 26.32%. And the electrical efficiency falls down by about 0.38%. The longer the co-axial tubular condenser, the larger the heat exchange area of the co-axial tubular condenser and the higher the thermal efficiency. A length of the co-axial tubular condenser between 3 m and 6 m recommends as a compromise between the efficiency of the system and the manufacturing costs.

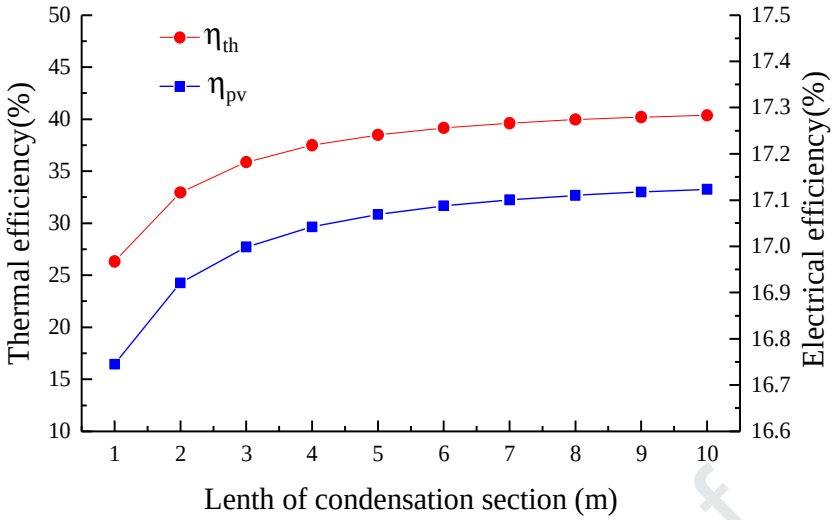

Fig. 25. Effects of different lengths of the co-axial tubular condenser on the thermal efficiency and electrical efficiency of the LHP- PV/T system.

5.3.6 Influence of simultaneous variation of the evaporator and the condenser region

A comparison between the influences of a reduced area in the evaporator on the LHP and IHP can be made. Unlike the LHP, the area ratio of the evaporator region to the condenser region of the IHP is fixed. Therefore, as the number of the heat pipes decreases, the areas of the evaporator and condenser region of the IHP both decreases, and may lead to considerable decrements in the thermal efficiency. The area ratio of the evaporator region to the condenser region in some commercial IHP solar system is about 8.3 [22, 24]. To conduct the simulation and comparison, this fixed area ratio is applied in the LHP- PV/T system. In this approximation, the results shall be applicable for an IHP-PV/T. The thermal and electrical performance under simultaneous variation of the evaporator and the condenser region is shown in Fig. 26. When the numbers of the heat pipes are 6, 12, 20, and 30, the lengths of the co-axial tubular condenser are 0.49 m, 0.98 m, 1.64 m, and 2.46 m. In contrast with that in Section 5.3.2, the lengths of the co-axial tubular condenser are variable and less than 5 m. As the number of heat pipes decreases from 30 to 6, the decrement in thermal efficiency is about 17.93%, from 35.15% to 17.22%, and the decrement in the electrical efficiency is about 0.47%, from 16.98%

to 16.51%. The influence of a reduced evaporator area on thermal and electrical efficiencies for an IHP-PV/T shall be much more significant than that on a LHP-PV/T, as compared with the results in Section 5.3.2. In other words, the LHP-PV/T can have fewer heat pipes for the evaporator with just a minor influence on efficiency.

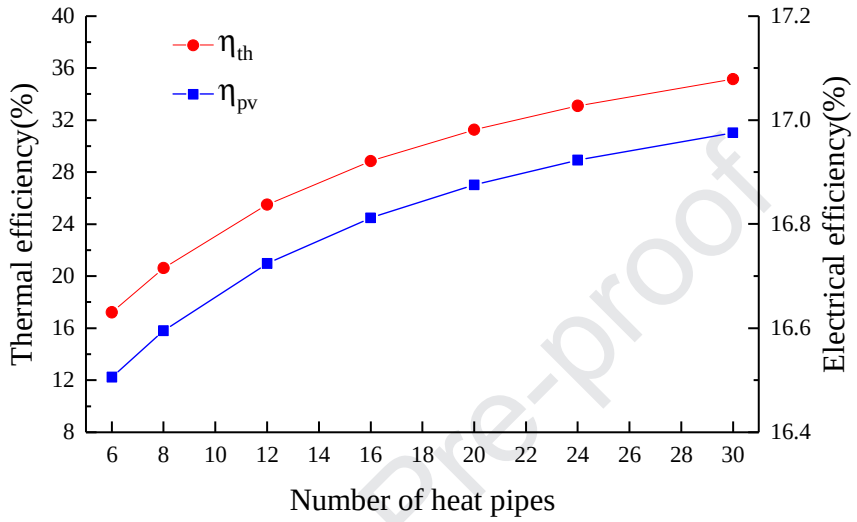

Fig. 26. Effects of simultaneous variation of the evaporator and the condenser region on the thermal efficiency and electrical efficiency of the LHP- PV/T system.

5.4 Potential for cost reduction

It is noteworthy that the micro-channel evaporator is crucial for the viability of the proposed LHP-PV/T. It has a high technical requirement, otherwise may suffer from leakage in the long term operation due to the fluctuating temperature of the PV/T. The micro-channels need to be laminated carefully on the absorber to avoid damage on the solar cells and encapsulation, and the manufacturing process is cumbersome. An area reduction in the micro-channel evaporator is desirable for the sake of technical feasibility and cost-effectiveness. The proposed system can potentially have much fewer heat pipes for the evaporator region without a significant efficiency decrement, as compared with a traditional IHP solar system. The latter generally has a restricted condenser section inside a manifold to diminish the heat loss and cost. The condenser section of the heat pipe has a high exergy destruction

rate due to the limited heat transfer area [10, 35]. The number of heat pipes is recommended to exceed 10 [36-38]. A lower number can lead to considerable decrements in both condensation and evaporation areas. Thermal efficiency is thereby remarkably affected. By contrast, a reduced evaporator area of the LHP of the proposed system is accompanied by a constant condensation area, and it shall just have a minor effect on the overall heat transfer performance because the thermal resistance of the evaporator is not predominant in the LHP- PV/T. The optimum number of heat pipes for the evaporator shall be lower than that for the IHP-PV/T.

In regard to the higher technical requirement and manufacturing costs than other components, optimization of the heat pipe for the evaporator is necessary. In this section, the potential of the LHP-PV/T system to reduce the manufacturing costs is assessed from the two aspects: the number of the heat pipe and the width of the heat pipe. Figs. 27 and 28 present the variations of the manufacturing costs under different numbers and widths of heat pipe. The two factors have a linear impact on manufacturing costs. When the number of heat pipe decreases from 30 to 6, and the thermal and electrical efficiencies of the LHP- PV/T system only drop by 4.63% and 0.12%, while the manufacturing costs can be reduced by 28.58%, from 1259.8 to 899.8 RMB. In addition, when the width of heat pipe is reduced from 26 mm to 10 mm, the thermal and electrical efficiencies are only decreased by 2.47% and 0.03%, whilst the manufacturing costs will be reduced by 21.45%, from 1243.1 to 976.5 RMB. Diminishing the number and width of heat pipe can potentially improve the cost-effectiveness of the proposed LHP- PV/T system.

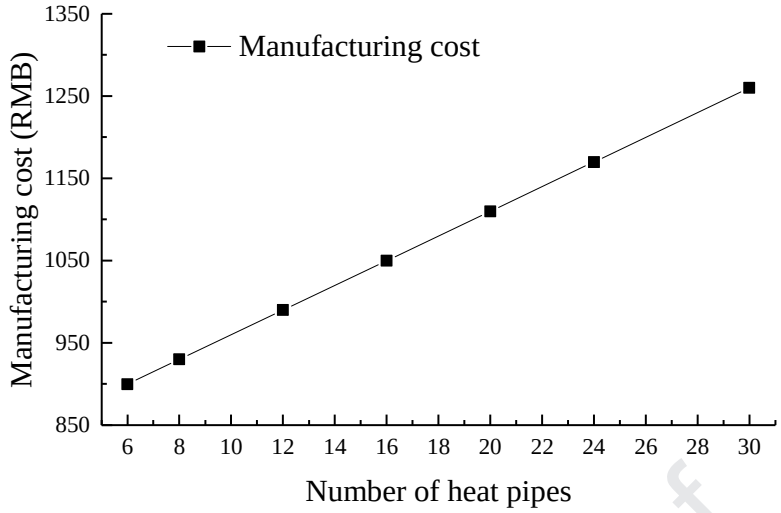

Fig. 27. Manufacturing costs under different numbers of heat pipes.

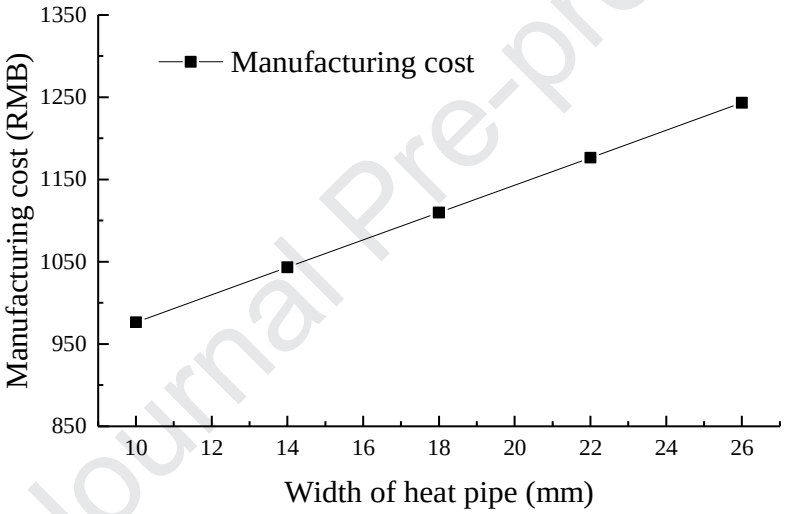

Fig. 28. Manufacturing costs under different widths of heat pipe.

6. Conclusions

This research addresses novel LHP- PV/T system which makes use of the co-axial tubular heat exchanger as the condenser, multiple micro-channel tubes arrays as the evaporator, the upper-end liquid header with tiny holes as the liquid feeder, and upper-end vapour header as the vapour collector and distributor. The co-axial tubular condenser can have sufficient length enabling full condensation of the working fluid and be coupled with the multiple evaporators. This design creates the single point

connection that can minimise the risk of leakage and facilitates the pressure maintain with the LHP. Moreover, the connection among the solar arrays becomes easier.

A dynamic distributed parameter model is developed. This model is applied to analyse the effects of various operational conditions on the performance of the LHP- PV/T system, as well as to optimise the geometrical and structural parameters. It is found that the modeling outcomes agree well with the experimental results, giving a discrepancy of less than 7.36%. With the decreases of the number and width of the heat pipe, both thermal and electrical efficiencies of the LHP- PV/T system decline. However, the decrements are not appreciable. The main reason is, the decrease of the evaporator area results in a larger thermal resistance between the working fluid and PV/T absorber but the enlarged thermal resistance is not predominant in the LHP- PV/T system.

The influence of the area reduction of the evaporator on LHP differs from that on the traditional IHP. For the former, the condenser section is unvaried as the evaporator area decreases, while for the latter, the condenser section decreases correspondingly due to the nature of IHP. The LHP- PV/T has more potential for cost reduction by diminishing the evaporator area, as compared with an IHP-PV/T.

When the number of the heat pipe is reduced from 30 to 6, the electrical efficiency is almost constant and the decrement in the thermal efficiency is about 4.63%. On the other hand, the system manufacturing cost drops by 28.58%. Through the optimization of the LHP evaporator which generally has a higher technical requirement and manufacturing cost than other components, the cost-effectiveness of the proposed LHP- PV/T system can be improved.

Acknowledgment

Sponsored by Innovate UK (TSB 70507-481546) for the Newton Fund – China-UK Research and Innovation Bridges Competition 2015 Project 'A High Efficiency, Low Cost and Building Integrate-able Solar Photovoltaic/Thermal (PV/T) System for Space Heating, Hot Water and Power Supply' and Dongguan Innovative Research Team Program (No. 2014607101008).

Appendix

This appendix is intended to show a clearer presentation of discretization in Section 3.2.

For the glass cover

$$d_{\mathrm{g}}\rho_{\mathrm{g}}c_{\mathrm{g}}\frac{T^{1}_{\mathrm{g}(i,j)}-T^{0}_{\mathrm{g}(i,j)}}{\Delta t}=d_{\mathrm{g}}\lambda_{\mathrm{g}}\frac{T^{1}_{\mathrm{g}(i+1,j)}-2T^{1}_{\mathrm{g}(i,j)}+T^{1}_{\mathrm{g}(i-1,j)}}{\Delta x^{2}}+d_{\mathrm{g}}\lambda_{\mathrm{g}}\frac{T^{1}_{\mathrm{g}(i,j+1)}-2T^{1}_{\mathrm{g}(i,j)}+T^{1}_{\mathrm{g}(i,j-1)}}{\Delta y^{2}}+h_{\mathrm{a}}(T_{\mathrm{a}}-T^{1}_{\mathrm{g}(i,j)})+h_{\mathrm{e,g}}(T_{\mathrm{e}}-T^{1}_{\mathrm{g}(i,j)})+(T^{1}_{\mathrm{pv}(i,j)}-T^{1}_{\mathrm{g}(i,j)})\big/R_{\mathrm{g,pv}}+G\alpha_{\mathrm{g}}. \tag{A1}$$

For the PV module

$$d_{\mathrm{pv}}\rho_{\mathrm{pv}}c_{\mathrm{pv}}\frac{T^{1}_{\mathrm{pv}(i,j)}-T^{0}_{\mathrm{pv}(i,j)}}{\Delta t}=d_{\mathrm{pv}}\lambda_{\mathrm{pv}}\frac{T^{1}_{\mathrm{pv}(i+1,j)}-2T^{1}_{\mathrm{pv}(i,j)}+T^{1}_{\mathrm{pv}(i-1,j)}}{\Delta x^{2}}+d_{\mathrm{pv}}\lambda_{\mathrm{pv}}\frac{T^{1}_{\mathrm{pv}(i,j+1)}-2T^{1}_{\mathrm{pv}(i,j)}+T^{1}_{\mathrm{pv}(i,j-1)}}{\Delta y^{2}}+\left(T^{1}_{\mathrm{g}(i,j)}-T^{1}_{\mathrm{pv}(i,j)}\right)\big/R_{\mathrm{g,pv}}+\left(T^{1}_{\mathrm{b}(i,j)}-T^{1}_{\mathrm{pv}(i,j)}\right)\big/R_{\mathrm{b,pv}}+G\left(\tau\alpha\right)_{\mathrm{pv}}-\xi E_{\mathrm{pv}}. \tag{A2}$$

For the connection nodes of the aluminum plate

$$d_{\mathrm{b}}\rho_{\mathrm{b}}c_{\mathrm{b}}\frac{T^{1}_{\mathrm{b}(i,j)}-T^{0}_{\mathrm{b}(i,j)}}{\Delta t}=d_{\mathrm{b}}\lambda_{\mathrm{b}}\frac{T^{1}_{\mathrm{b}(i+1,j)}-2T^{1}_{\mathrm{b}(i,j)}+T^{1}_{\mathrm{b}(i-1,j)}}{\Delta x^{2}}+d_{\mathrm{b}}\lambda_{\mathrm{b}}\frac{T^{1}_{\mathrm{b}(i,j+1)}-2T^{1}_{\mathrm{b}(i,j)}+T^{1}_{\mathrm{b}(i,j-1)}}{\Delta y^{2}}+\left(T^{1}_{\mathrm{pv}(i,j)}-T^{1}_{\mathrm{b}(i,j)}\right)\big/R_{\mathrm{b,pv}}+\left(T^{1}_{\mathrm{h}(i,j-n)}-T^{1}_{\mathrm{b}(i,j)}\right)\big/R_{\mathrm{b,h}}. \tag{A3}$$

where "n" is the difference between the number of the nodes on the y-axis of the aluminum plate and

the heat pipe.

For the middle nodes of the aluminum plate

$$d_{\mathrm{b}}\rho_{\mathrm{b}}c_{\mathrm{b}}\frac{T^{1}_{\mathrm{b}(i,j)}-T^{0}_{\mathrm{b}(i,j)}}{\Delta t}=d_{\mathrm{b}}\lambda_{\mathrm{b}}\frac{T^{1}_{\mathrm{b}(i+1,j)}-2T^{1}_{\mathrm{b}(i,j)}+T^{1}_{\mathrm{b}(i-1,j)}}{\Delta x^{2}}+d_{\mathrm{b}}\lambda_{\mathrm{b}}\frac{T^{1}_{\mathrm{b}(i,j+1)}-2T^{1}_{\mathrm{b}(i,j)}+T^{1}_{\mathrm{b}(i,j-1)}}{\Delta y^{2}}+\left(T^{1}_{\mathrm{pv}(i,j)}-T^{1}_{\mathrm{b}(i,j)}\right)\Big/R_{\mathrm{b,pv}}+\left(T_{\mathrm{a}}-T^{1}_{\mathrm{b}(i,j)}\right)\Big/R_{\mathrm{b,a}}\quad(\mathrm{A4})$$

For the MCHP shell

$$d_{\mathrm{h}}\rho_{\mathrm{h}}c_{\mathrm{h}}\frac{T^{1}_{\mathrm{h}(i,j)}-T^{0}_{\mathrm{h}(i,j)}}{\Delta t}=d_{\mathrm{h}}\lambda_{\mathrm{h}}\frac{T^{1}_{\mathrm{h}(i+1,j)}-2T^{1}_{\mathrm{h}(i,j)}+T^{1}_{\mathrm{h}(i-1,j)}}{\Delta x^{2}}+d_{\mathrm{h}}\lambda_{\mathrm{h}}\frac{T^{1}_{\mathrm{h}(i,j+1)}-2T^{1}_{\mathrm{h}(i,j)}+T^{1}_{\mathrm{h}(i,j-1)}}{\Delta y^{2}}+h_{\mathrm{r,h}(i,j)}\left(T^{1}_{r}-T^{1}_{\mathrm{h}(i,j)}\right)+\left(T^{1}_{b(i,j+n)}-T^{1}_{\mathrm{h}(i,j)}\right)\Big/R_{\mathrm{b,h}}+\left(T_{\mathrm{a}}-T^{1}_{\mathrm{h}(i,j)}\right)\Big/R_{\mathrm{h,a}}\quad(\mathrm{A5})$$

For all the working fluid

$$M_{\mathrm{r}}c_{\mathrm{r}}\frac{T^{1}_{\mathrm{r}}-T^{0}_{\mathrm{r}}}{\Delta t}=\sum A_{\mathrm{r,h,ij}}h_{\mathrm{r,h}(i,j)}\left(T^{1}_{\mathrm{h}(i,j)}-T^{1}_{\mathrm{r}}\right)+\sum A_{\mathrm{r,t,ij}}h_{\mathrm{r,t}(i,1)}\left(T^{1}_{\mathrm{t}(i,j)}-T^{1}_{\mathrm{r}}\right).\quad(\mathrm{A6})$$

For the inner tube shell in the condenser section

$$A_{\mathrm{t}}\rho_{\mathrm{t}}c_{\mathrm{t}}\frac{T^{1}_{\mathrm{t}(i,1)}-T^{0}_{\mathrm{t}(i,1)}}{\Delta t}=A_{\mathrm{t}}\lambda_{\mathrm{t}}\frac{T^{1}_{\mathrm{t}(i+1,1)}-2T^{1}_{\mathrm{t}(i,1)}+T^{1}_{\mathrm{t}(i-1,1)}}{\Delta x^{2}}+P_{\mathrm{t,out}}h_{\mathrm{w,t}}(T^{1}_{\mathrm{w}(i,1)}-T^{1}_{\mathrm{t}(i,1)})+P_{\mathrm{t,in}}h_{\mathrm{r,t}(i,1)}(T^{1}_{\mathrm{r}}-T^{1}_{\mathrm{t}(i,1)}).\quad(\mathrm{A7})$$

For the flowing water in the condenser section

$$A_{\mathrm{w}}\rho_{\mathrm{w}}c_{\mathrm{w}}\frac{T^{1}_{\mathrm{w}(i,1)}-T^{0}_{\mathrm{w}(i,1)}}{\Delta t}=-\dot{M}_{\mathrm{w}}c_{\mathrm{w}}\frac{T^{1}_{\mathrm{w}(i-2,1)}-4T^{1}_{\mathrm{w}(i-1,1)}+3T^{1}_{\mathrm{w}(i,1)}}{2\Delta x}+A_{\mathrm{w}}\lambda_{\mathrm{w}}\frac{T^{1}_{\mathrm{w}(i+1,1)}-2T^{1}_{\mathrm{w}(i,1)}+T^{1}_{\mathrm{w}(i-1,1)}}{\Delta x^{2}}+P_{\mathrm{t,out}}h_{\mathrm{w,t}}\left(T^{1}_{\mathrm{t}(i,1)}-T^{1}_{\mathrm{w}(i,1)}\right)\quad(\mathrm{A8})$$

In these equations, the superscript “0” represents the results of the previous time step and “1” refers

to the results of the current time step.

References

[1] Launay S, Sartre V, Bonjour J. Parametric analysis of loop heat pipe operation: a literature review. Int J Therm Sci 2007; 46. 621-636.

[2] Yu. F. Maydanik. Loop heat pipes. Appl. Therm. Eng. 2005; 25: 635-657.

[3] K Goncharov, V. Kolesnikov. Development of propylene LHP for spacecraft thermal control systems. in: Proc. of 12th Int. Heat Pipe Conference, Moscow, Russia, 2002: 171-176.

[4] C.L. Baker, E.W. Grob, T.V. McCarthy, M.N. Nikitkin, W.C. Ancarrow. Geoscience laser altimetry system (GLAS) on-orbit flight report on the propylene loop heat pipes (LHPs). in: Proc. of Int. Two-Phase Thermal-Control Technology Workshop, Noordwijk, Netherlands, 2003;699: 88-95.

[5] C.S. Chang, B.J. Huang, Yu.F. Maydanik. Feasibility of a mini LHP for CPU cooling of a Notebook PC. in: Proc. of 12th Int. Heat Pipe Conference, Moscow, Russia, 2002: 390-393.

[6] V.G. Pastukhov, Yu.F. Maydanik, C.V. Vershinin, M.A. Korukov. Miniature loop heat pipes for electronic cooling. Appl. Therm. Eng. 2003; 23: 1125-1135.

[7] Zhangyuan Wang, Wansheng Yang. A review on loop heat pipe for use in solar water heating. Energy and Buildings 2014; 79: 143-154.

[8] R.S. Soin, K. Sangameswar Rao, D.P. Rao, K.S. Rao. Performance of a flat plate solar collector with fluid undergoing phase change. Sol. Energy 1979; 23: 69-73.

[9] Behrooz M. Ziapour, Naser Yadgari Kheljan, Mohsen Bagheri Khalili. Performance study of solar water heater comprised of the separate loops flow boiling in the mini tubes. Energy

Convers Manage 2016; 111: 245-252.

[10] Ziapour BM, Shaker H. Exergetic analysis of a long two-phase closed thermosyphon system. Int J Exergy 2010; 7: 714-30.

[11] Pei Gang, Fu Huide, Zhu Huijuan, Ji Jie. Performance study and parametric analysis of a novel heat pipe PV/T system. Energy 2012; 37:384-395.

[12] X. Zhao, Z. Wang, Q. Tang. Theoretical investigation of the performance of a novel loop heat pipe solar water heating system for use in Beijing, China. Appl. Therm. Eng. 2010; 30: 2526-2536.

[13] X. Zhang, X. Zhao, J. Xu, X. Yu. Characterization of a solar photovoltaic/loop heat-pipe heat pump water heating system. Appl. Energy 2013; 102: 1229-1245.

[14] X. Zhang, X. Zhao, J. Shen, X. Hu, X. Liu, J. Xu. Design, fabrication and experimental study of a solar photovoltaic/loop-heat-pipe based heat pump system. Sol. Energy 2013; 97: 551-568.

[15] Ji Li, Feng Lin, Gengwen Niu. An insert-type two-phase closed loop thermosyphon for split-type solar water heaters. Appl. Therm. Eng. 2014; 70: 441-450.

[16] N.Z. Aung, S. Li. Numerical investigation on effect of riser diameter and inclination on system parameters in a two-phase closed loop thermosyphon solar water heater. Energy Convers Manage 2013; 75: 25-35.

[17] Wei He, Xiaoqiang Hong, Xudong Zhao, Xingxing Zhang, Jinchun Shen, Jie Ji. Operational performance of a novel heat pump assisted solar façade loop-heat-pipe water heating system. Appl. Energy 2015; 146: 371-382.

[18] M.A. Ebadian, C.X. Lin. A review of high-heat-flux heat removal technologies. J. Heat Transfer 2011; 133(11): 110801.

[19] Ling Li, Zhang Quan, Yu Yuebin, Wu Yaning, Liao Shuguang. Study on thermal performance of micro-channel separate heat pipe for telecommunication stations: experiment and simulation. International Journal of Refrigeration 2015; 59:198-209.

[20] Y.H. Diao, L. Liang, Y.M. Kang, Y.H. Zhao, Z.Y. Wang, T.T. Zhu. Experimental study on the heat recovery characteristic of a heat exchanger based on a flat micro-heat pipe array for the ventilation of residential buildings. Energy and Buildings 2017; 152: 448-457.

[21] Y. H. Diao, S. Wang, C. S. Li, Y. H. Zhao, T. T. Zhu. Experimental study on the heat-transfer characteristics of a new-type flat micro-heat-pipe heat exchanger with latent heat thermal energy storage. Experimental Heat Transfer 2016; 30: 91-111.

[22] Yuechao Deng, Yaohua Zhao, Wei Wang, Zhenhua Quan, Lincheng Wang, Dan Yu. Experimental investigation of performance for the novel flat plate solar collector with MCHP array (MHPA-FPC). Appl. Therm. Eng. 2013; 54: 440-449.

[23] Zhu T, Diao Y, Zhao Y, Li F. Thermal performance of a new CPC solar air collector with flat micro-heat pipe arrays. Appl. Therm. Eng. 2016; 98: 1201-1213.

[24] Longshu Hou, Zhenhua Quan, Yaohua Zhao, Lincheng Wang, Gang Wang. An experimental and simulative study on a novel photovoltaic-thermal collector with micro heat pipe array (MHPA-PV/T). Energy and Buildings 2016; 124:60-69.

[25] Modjinou M, Ji J, Li J, Yuan W, Zhou F. A numerical and experimental study of micro-channel heat pipe solar photovoltaics thermal system. Appl. Energy 2017; 206: 708-22.

[26] Zhou J, Zhao Z, Ma X, Zhu Z, Qiu Z, Ji J, Du Z Yu M. Experimental investigation of a solar driven direct-expansion heat pump system employing the novel PV/micro-channels-evaporator modules. Appl. Energy 2016; 178: 484-495.

[27] Tao Zhang, Gang Pei, Qunzhi Zhu, Jie Ji. Investigation on the optimum volume-filling ratio of a loop thermosyphon solar water-heating system. J. Sol. Energy Eng 2016; 138(4): 041006.

[28] E. Mathioulakis, V. Belessiotis. A new heat-pipe type solar domestic hot water system. Sol. Energy 2002; 72: 13-20.

[29] M.Yu, T.M.O.Diallo, X.D. Zhao, J.Z. Zhou, Z.Y. Du, J. Ji, Y.D. Cheng. Analytical study of impact of the wick's fractal parameters on the heat transfer capacity of a novel micro-channel loop heat pipe. Energy 2018; 158: 746-759.

[30] Thierno M.O. Diallo, Min Yu, Jinzhi Zhou, Xudong Zhao, Samson Shittu,Guiqiang Li, Jie Ji, David Hardy. Energy performance analysis of a novel solar PVT loop heat pipe employing a microchannel heat pipe evaporator and a PCM triple heat exchanger. Energy 2019; 167: 866-888.

[31] Sung-Min Kim, Issam Mudawar. Universal approach to predicting saturated flow boiling heat transfer in mini/micro-channels – Part II. Two-phase heat transfer coefficient. International Journal of Heat and Mass Transfer 2013; 64:1239-1256.

[32] M.K. Dobson, J.C. Chato. Condensation in smooth horizontal tubes. Journal of Heat Transfer 1998; 120: 193-213.

[33] ANSI/ASHRAE 93-2010 Methods of testing to determine the thermal performance of solar collectors. New York: ASHRAE; 2010.

[34] http://www.fivestarsolar.com/.

[35] Farzad JAFARKAZEMI, Emad AHMADIFARD, Hossein ABDI. Energy and exergy efficiency of heat pipe evacuated tube solar collectors. Thermal Science 2016; 20(1): 327-335.

[36] J. R. Hull. Analysis of heat transfer factors for a heat pipe absorber array connected to a common

manifold. Journal of Solar Energy Engineering 1986; 108 (1):11-16.

[37] H.M.S. Hussein. Theoretical and experimental investigation of wickless heat pipes flat plate solar collector with cross flow heat exchanger. Energy Convers Manage 2007; 48: 1266-1272.

[38] E. Azad. Experimental analysis of thermal performance of solar collectors with different numbers of heat pipes versus a flow-through solar collector. Renewable and Sustainable Energy Reviews 2018; 82: 4320-4325.

1. A novel loop heat pipe solar photovoltaic/thermal system is built.

2. An accurate distributed parameter model is developed.

3. Cost reduction potential of the system is investigated.

4. Influences of a reduced evaporator area on LHP differ from those on IHP.

5. The system cost is reduced by 28.58% with a minor decrement in the performance.